AD A 108 045

Stress Corrosion of Ceramic Materials

S. W. Freiman, et al

Technical Report

ONR Contract No. N00014-79F-0030
NBS Project No 5620454
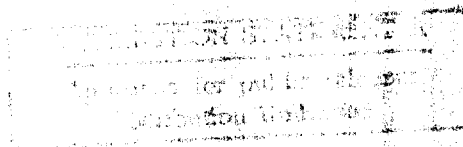
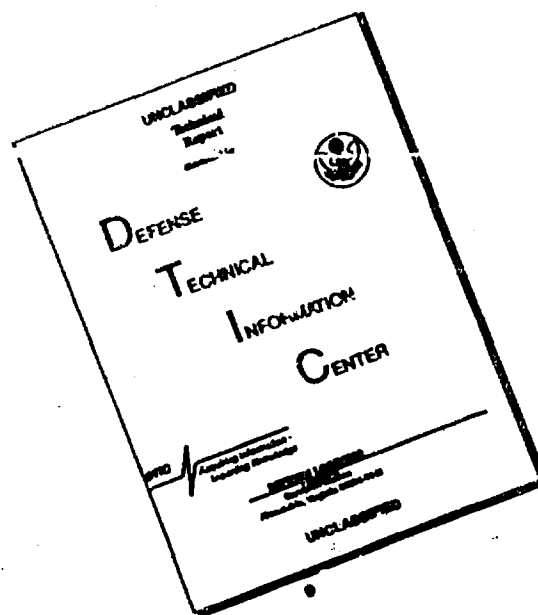For

Office of Naval Research
Arlington, VA 22217

by

National Bureau of Standards
Washington, DC 20234

October 1981

DISCLAIMER NOTICE

THIS DOCUMENT IS BEST
QUALITY AVAILABLE. THE COPY
FURNISHED TO DTIC CONTAINED
A SIGNIFICANT NUMBER OF
PAGES WHICH DO NOT
REPRODUCE LEGIBLY.

FOREWORD

This report describes the results of an experimental program to investigate mechanisms of stress corrosion in glasses and ceramics and to determine effects of composition and microstructure on the fracture of piezoelectric materials.

Table of Contents

Accession For

NTIS GRA&I	☑
DTIC TAB	☐
Unannounced	☐
Justification	

By
Distribution/
Availability Codes
Avail and/or
Dist Special

INTRODUCTION

One of the main reasons for strength degradation of structural ceramic materials is stress corrosion cracking. Caused mainly by water in the environment, stress corrosion cracking results in subcritical crack growth that leads to delayed failure of ceramic materials. As a consequence of this crack growth, ceramic components that are subjected to external stresses are liable to fail after an indeterminate period of time, leading to a considerable uncertainty in the safe design stress. One of the objectives of modern ceramics technology is to reduce the uncertainty associated with structural design, and hence, to improve our capabilities of designing ceramic components that exhibit reliable mechanical behavior. This objective can be accomplished in part through a better understanding of the fundamental processes that occur during stress corrosion cracking.

Recent advances in the area of structural design with ceramic materials have lead to several new procedures for evaluating materials performance so that lifetime under load can be predicted. These techniques are all based on the science of fracture mechanics, which provides a theoretical basis for understanding how crack growth leads to structural failure. Fruitful use of these techniques requires that crack growth behavior of a material be characterized so that long term strength behavior can be predicted. This characterization can be accomplished either by the use of fracture mechanics techniques (measurement of crack velocity as a function of stress intensity factor), or by the use of strength techniques (e.g. stress-rupture experiments). Current studies on the subject of stress corrosion cracking indicate a pressing need for basic research to elucidate the chemical and physical processes that are pertinent to the process of stress corrosion cracking. This information could then be used to develop basic models which would improve our

i

capability of making long term failure predictions for specific engineering applications.

Our present state of understanding of stress corrosion cracking of glass and other ceramics is primitive in the sense that although water is known to be the main stress corrosion agent, the actual chemical reactions causing the stress corrosion cracking are virtually unknown. Hence, while we can measure crack growth rates, or strength degradation rates for specific ceramic materials, our lack of knowledge of stress corrosion mechanisms, prevents us from selecting materials compositions, or microstructures that have a maximum resistance to crack growth. This same lack of knowledge prevents us from applying fracture mechanics theory to predict component lifetime, when the lifetime required greatly exceeds certain time limits established by the experimental crack growth or stress rupture data. The work reported herein was obtained as part of a program designed to further our understanding of the stress corrosion mechanism.

A MOLECULAR INTERPRETATION OF STRESS CORROSION IN SILICA

by

Terry A. Michalske
and
Stephen W. Freiman

Fracture and Deformation Division
National Bureau of Standards
Washington, D.C.   20234

Abstract

The mechanical strength of many glasses and ceramic materials decreases with time under static loading and ambient environments. This strength loss is associated with slow growth of pre-existing surface flaws due to stress-corrosion by water from the surrounding environment. In order to make strength predictions for ceramic components with long term applications, it becomes necessary to understand the mechanism by which this stress-corrosion occurs. We have studied stress-corrosion in vitreous silica exposed to water and several non-aqueous environments and report here that environments which enhance stress-corrosion crack growth contain active groups with electron donor sites on one end and proton donor sites at the other. These results suggest a detailed chemical model for the interaction of the environment with mechanically strained bonds in the solid at the tip of a crack. The proposed model for stress-corrosion crack growth also has implications for the long term strength behavior of a wide variety of brittle materials.

Previously published results[1] have shown that slow extension ($<10^{-2}$ m/s) of a crack in vitreous silica is facilitated by water in the environment. This effect can be demonstrated in a plot of crack velocity (V) versus stress intensity factor (K_I), where K_I is a measure of the stress field concentrated by the crack tip. Crack velocities were obtained by visual observation of crack extension in a double cantilever beam type specimen. The important features of such a plot for vitreous silica (Figure 1) are:

(1) In a water free environment such as vacuum, spontaneous failure is observed when K_I reaches a critical value.

(2) When small amounts of water vapor are introduced, crack growth in the low velocity regime is enhanced (curve is shifted to lower K_I and V is a measurable function of K_I). The relative amount of enhancement is related to the chemical activity of water in the environment.[2]

(3) A plateau in crack velocity is observed in water containing environments (e.g. moist N_2). This plateau has been linked to crack growth limited by the rate of water transport to the tip of the moving crack.[2] At sufficiently high V the plateau behavior ends and rapid fracture is observed.

(4) Liquid water enhances crack growth over the entire range of crack velocity ($10^{-9} - 10^{-2}$).

Several generalized mechanisms have been proposed to explain the effect of water containing environments on crack growth in glass. Orowan[3] suggested that the environment could reduce the energy of the fracture generated surface thereby creating a more energetically favorable process for cracking. Charles and Hillig[4] have discussed stress enhanced dissolution of material at the crack tip and its effect on the strength of alkali silicate glass. Finally, Wiederhorn[5] used dielectric charge

- 1 -

compensation in a model to explain environmentally enhanced fracture of glass. This communication will describe, on a molecular scale, a specific chemical reaction between strained bonds in vitreous silica and water which can be used to explain environmentally enhanced crack growth. Experimental results in support of this model will also be presented.

Since we wish to present a molecular picture of the chemical reaction leading to fracture, a brief description of the structure and bonding in the solid and the environment is in order.

Network silicates (quartz, coesite, vitreous silica, etc.) are composed of $[SiO_4]^{-4}$ tetrahedral units linked at their corners by shared or bridging oxygen atoms $(O_{(br)})$. On an atomic scale, the bridging Si – O – Si bond is the stress supporting member of the structure and will be important to the fracture process. Although some controversy remains over the exact nature of the bridging bond, recent ab-initio MO calculations[6] for orthosilicic and pyrosilicic acids indicate that both σ-bonds and π-bonds are formed. It is suggested that an sp^3 hybrid orbital from Si σ-bonds with an $(s + \lambda p_z)$ hybrid from $O_{(br)}$ and that lone pair px and py orbitals from $O_{(br)}$ are involved in π-bonding with all five d orbitals from Si. These results are in good agreement with experimental measurements for ortho and pyrosilicic acids as well as network silicates.

At the crack tip in a stressed solid, highly concentrated stress fields are produced. Continuum approximations[5] indicate that the bridging bond experiences strains >20%. The effect of this strain on the bonding molecular orbitals is not easy to predict but can be discussed in terms of a decrease in the overlap between atomic orbitals thus increasing their availability for bonding with other species.

The structure and bonding in the water molecule is established in the literature. Oxygen atomic orbitals 2s, 2px and 2py form three hybrid orbitals two of which σ-bond with hydrogen atoms. The remaining lone pair orbitals (one hybrid and the remaining pz) are directed away from the hydrogen atoms. This arrangement results in a positive charge center at the hydrogen end of the water molecule and a negative charge center on the opposite end of the molecule where the lone pair orbitals are located.

Interaction between strained bridging bonds in silica and water from the environment can be represented by a three step process (see Fig. 2).

Step 1 – A water molecule from the environment attaches to a bridging Si–O–Si bond at the crack tip. The water molecule is aligned by:

1) formation of a hydrogen bond with the $O_{(br)}$ atom and

2) interaction of the lone pair orbitals from $O_{(w)}$ with the Si atom. The lone pair orbital interaction may involve either Van der Waals attraction or some covalent bonding with unoccupied d orbitals of Si.

Step 2 – A concerted reaction occurs in which proton transfer to the $O_{(br)}$ is accomplished simultaneously with electron transfer from the $O_{(w)}$ to the Si atom. As a result of this reaction, two new bonds are formed (one between $O_{(w)}$ and Si, and one between hydrogen and $O_{(br)}$; the original briding bond (between $O_{(br)}$ and Si) is destroyed.

Step 3 – Rupture of the hydrogen bond between $O_{(w)}$ and transferred hydrogen occurs to yield surface Si–O–H groups on each fracture surface. Since the hydrogen bond is weak, this step is expected to

occur immediately after proton transfer. (Budd[7] has proposed a similar mechanism for the dissolution of slica in water, however, it should be noted that the present model for crack growth is not contingent on the removal of material from the fracture surface).

Reaction rate theory[8] can be used to show how the proposed mechanism for bond rupture leads to enhanced crack growth rates. In vacuum, the entire energy of the bridging bond must be overcome before bond rupture can occur. (This energy is supplied in part by mechanical strain as well as by thermal contributions). When water is present, the height of the energy barrier to bond rupture is reduced because charge transfer (Step 2) provides an alternate, lower energy, reaction path. Accordingly, the activated complex is that structure which exists during the charge transfer reaction. Since the rate of a chemical reaction (in this case bond rupture) is reciprocally dependent on the exponent of the energy barrier, mechanisms that provide a lower energy activated state will enhance crack growth rates. This brief discussion has omitted factors resulting from changes in the energy of the Si-O-Si bond due to adsorbed water (Step 1) and the energy of the reaction products (Step 3); these terms are not critical to this communication and will be presented in detail elsewhere.

Experimentally, the role of the concerted reaction (simultaneous electron and proton transfer) as the rate of limiting step to fracture can be born out through isotopic effects. Results of fracture experiments performed in deuterated water produced crack velocities consistently lower than those attained in normal water. This result can be analyzed in terms of the different ground state vibrational energies of deuterium and protium resulting in different activation barriers for the two isotopes. The lower rack velocities measured in deuterated water are in agreement th the larger energy barrier expected for deuteron transfer.[9]

- 4 -

This model for chemical bond rupture presents a number of interesting implications. First, it suggests that environments other than water should enhance cracking in silica glass if the species possess structural and bonding features similar to water i.e. proton donor sites at one end of the molecule (or group) and lone pair orbitals at the other. The environmental molecule must also fit between the Si-O bond ($\sim$1.63 Å). To test this hypothesis, crack growth studies were conducted in vitreous silica exposed to ammonia (NH_3). Ammonia has a structure similar to water except that it has three orbitals σ-bonded to hydrogens leaving one lone pair orbital directed away from the hydrogen atoms (the N-H bond length is 0.94 Å). Figure 3 shows that indeed, NH_3 enhanced crack growth over the entire velocity range. When evaluating such data it is important to be aware that small amounts of water in an inert carrier (N_2) can have large effects on crack growth rates. However, as previously discussed, the enhancement due to small amounts of water is limited in velocity. Since the NH_3 gas used in this experiment contained less H_2O than the $N_2 + H_2O$ gas mixture, the absence of a plateau indicates that the NH_3 was controlling the fracture behavior. Crack growth experiments in hydrazine (N_2H_4) and formamide (CH_3NO) showed that these environments also controlled crack growth over the entire velocity range. However, these environments were less effective (V-K_I curve shifted to higher K_I) then either water or ammonia possibly due to steric hinderence and/or delocalization of lone pair orbitals. It is also noteworthy that other non-aqueous environments such as carbon monoxide (contains lone pair orbital but no proton donor site) or acetonitrile (has high dipole moment, 3.92D, but no localized lone pair orbital) have no measureable effect on crack growth rates.

The model also suggests that environmentally enhanced crack growth of this type can only occur in solids containing structural bonds between

proton acceptors and electron acceptors. Crack growth measurements in single crystal Si suggest little if any effect of water on crack growth rates,[10] which is in agreement with this hypothesis.

Finally, information suggested by this model can conceivably be applied to calculations of reaction rates for the bond rupturing process. In order to make such calculations (either by semi-empirical or ab-initio methods) geometries of the reactants and activated complex must be known. The most difficult procedure involves determination of the activated complex since it does not exist for finite times and cannot be measured spectroscopically. Our model of the bond rupturing process does suggest a possible geometry for the activated complex (Step 2 of Fig. 2) which may be useful in such calculations. Further details concerning such calculations and their application to predictions for fracture behavior will be presented elsewhere.
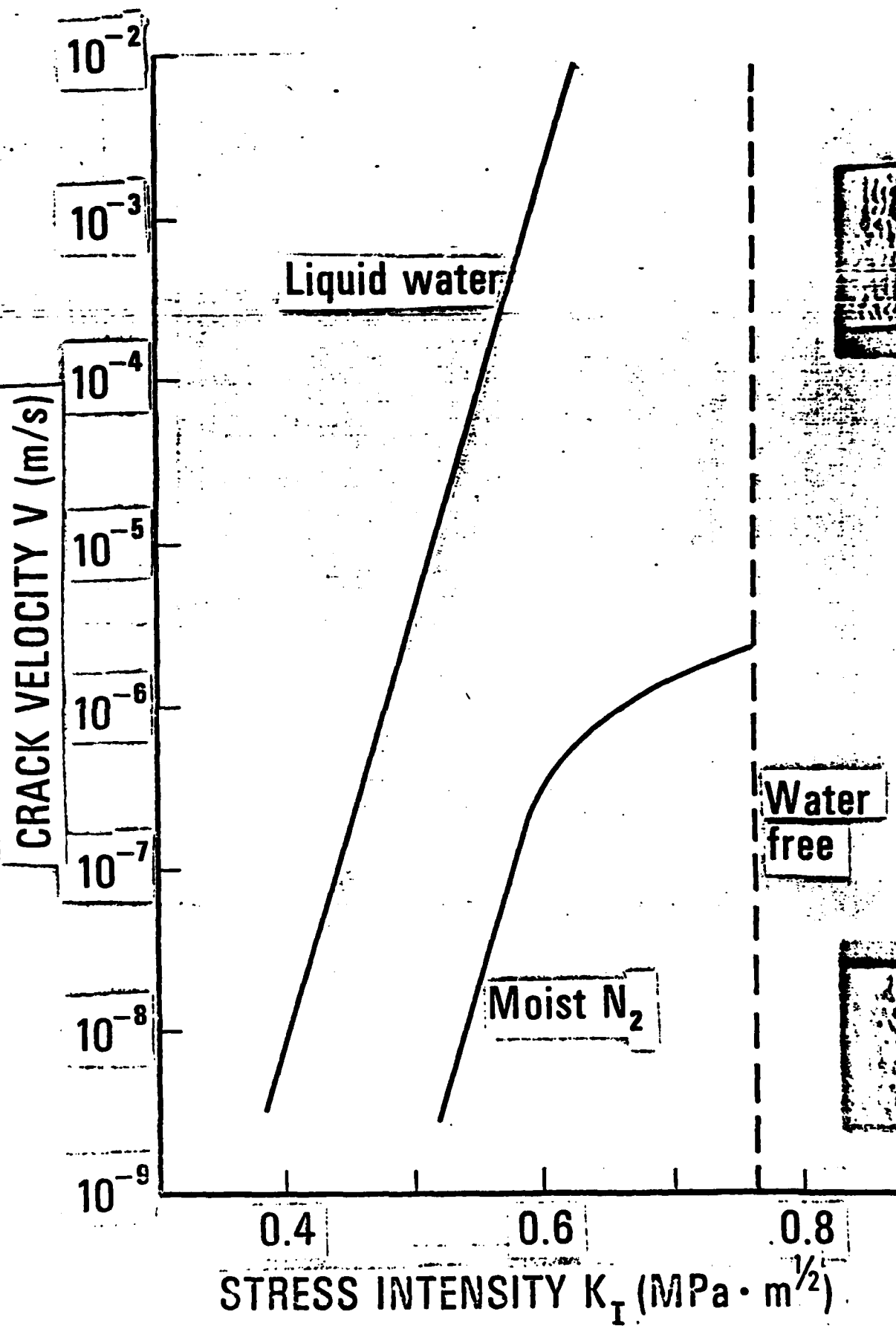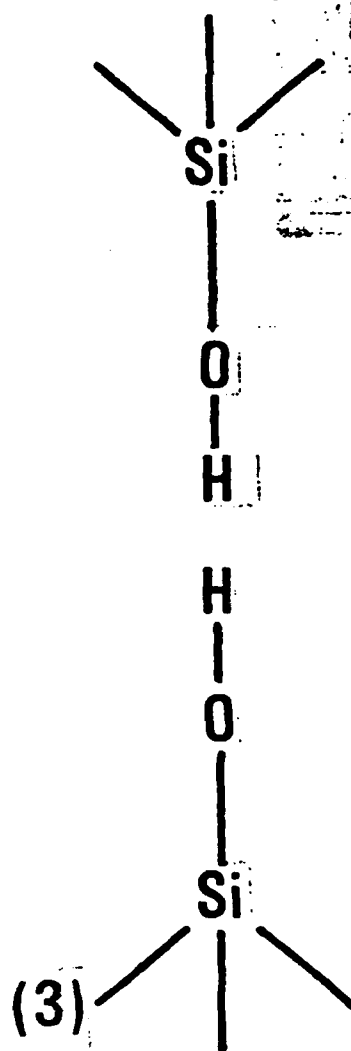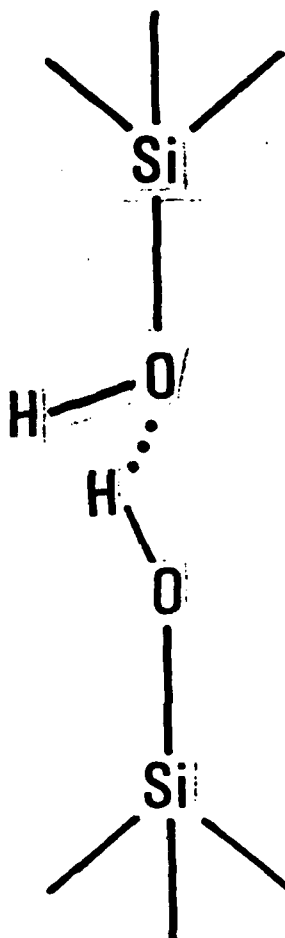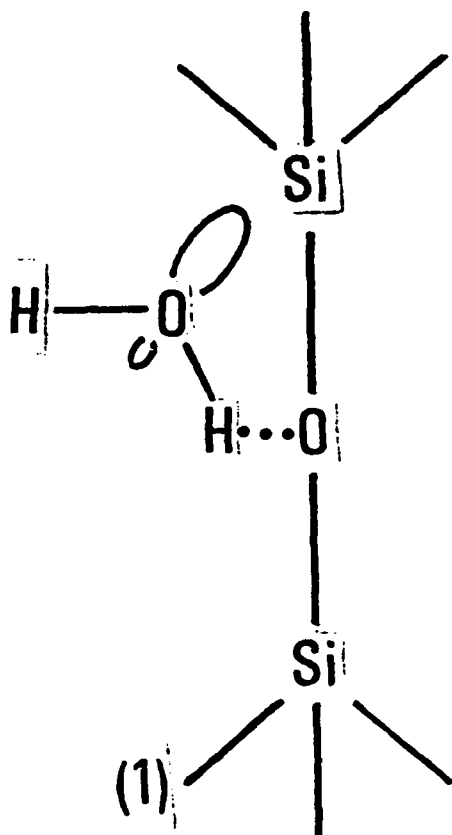
References

1. Wiederhorn, S.M. and Bolz, C.H., J. Am. Ceram. Soc. <u>53</u>, 543 (1970).

2. Wiederhorn, S.M. in Fracture Mechanics of Ceramics Vol. 4 (ed. Bradt, R.C., Hasselman, D.P.H., and Lange, F.F.) 549 (Plenum, New York, 1978).

3. Orowan, E., Nature, <u>154</u>, 341 (1944).

4. Hillig, W.B. and Charles, R.J. in High Strength Materials 682 (ed. Zackay, V.F.) 682 (Wiley, New York, 1965).

5. Wiederhorn, S.M. Fuller, E.R., Jr. and Thomson, R., Metal Science, <u>14</u>, 450 (1980).

6. Newton, M.D. and Gibbs, G.V. Physics and Chemistry of Minerals, <u>6</u>, 221 (1980).

7. Budd, S.M., Phys. Chem. Glass, <u>2</u>, 111 (1961).
8. Laidler, K.J. Theories of Chemical Reaction Rates (McGrawHill, New York, 1969).

9. Melander, L. and Saunders, W.H. Reaction Rates of Isotopic Molecules (Wiley and Sons, New York, 1980).

10. Fuller, E.R. personal communication (1980).

Figure 1. Effect of water on slow crack growth in vitreous silica (curves
represent best fit to experimental data).

Figure 2. Schematic representation of the proposed reaction between water
and a strained Si-O-Si bond at the crack tip. Reaction steps
involve; (1) adsorbtion of water to Si-O bond, (2) concerted
reaction involving simultaneous proton and electron transfer
and (3) formation of surface hydroxyls.

Figure 3. Comparison of the effects of water and ammonia on slow crack
growth in vitreous silica at room temperature.
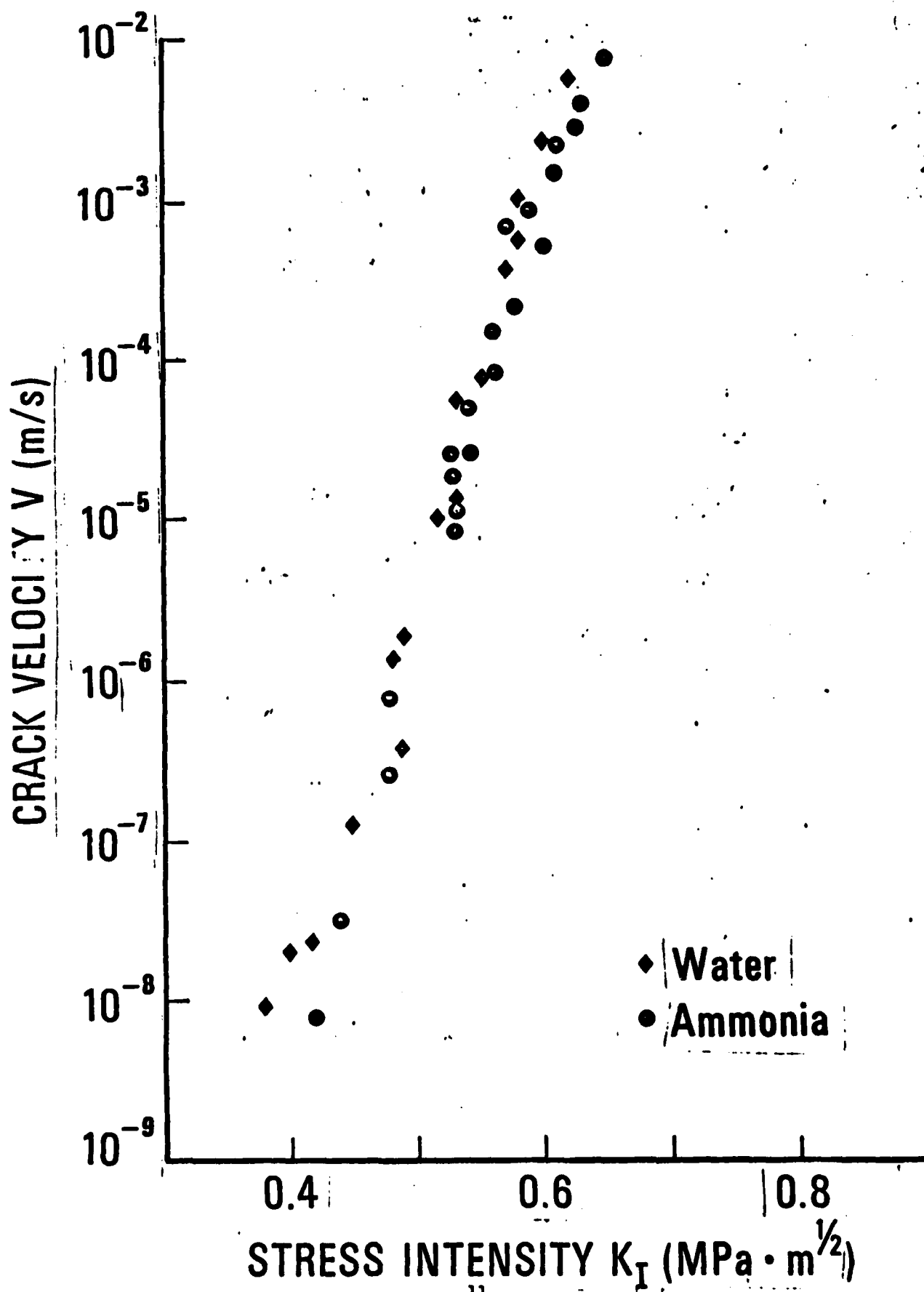
CRACK VELOCITY V (m/s)

STRESS INTENSITY K_I (MPa·m$^{1/2}$)

Liquid water

Moist N_2

Water free

- 9 -

(1)

(3)

Friiman

- 11 -

Effect of Corrosion Processes on Subcritical Crack Growth in Glass

C. J. Simmons[+] and S. W. Freiman
Fracture and Deformation Division
National Bureau of Standards
Washington, D.C. 20234

Abstract

Crack growth studies were conducted on soda lime silica, soda borosilicate and two binary soda silica glasses immersed in solutions of 1 Molar Li^+, 1 Molar Cs^+ or deionized water at different pH values. A definite effect of the Li^+ and Cs^+ was observed on the V-K_I curves in all but the soda lime glass. A plateau in crack velocity in the range 10^{-8} to 10^{-10} m/sec was measured on the binary soda-silica glasses for $K_I < 0.35$ $MPam^{1/2}$. These data are analyzed in terms of both the ion exchange and SiO_2 dissolution steps of the corrosion process. A model of crack growth in corrosive conditions is proposed.

[+]Now at the Vitreous State Laboratory, Catholic University of America, Washington, D.C. 20064

Effect of Corrosion Processes on Subcritical Crack Growth in Glass

C. J. Simmons and S. W. Freiman

Introduction

Logarithmic plots of crack velocity versus stress intensity, K_I, for glasses in moist environments typically have three regions of behavior, a portion with a slope of 10 to 40, a nearly flat portion, and a steep, water independent part. Crack growth in region I, $\sim 10^{-10} - 10^{-4}$ m/sec. is governed by the rate of reaction of the material with water in the environment[1]. It is to this region that this study is addressed. It is observed that the slope and position of the crack velocity vs. K_I curves in region I are affected by glass composition,[2] the partial pressure of water in other media,[3] and the pH of aqueous solutions[4]. However, a more direct link between corrosion rates of glasses and crack growth behavior has not been established.

Glass corrosion occurs by two processes:[5]

1) Exchange of alkali ions in the glass with hydrogen ions from the enviornment.

2) Hydrolysis of the Si-O bonds leading to dissolution of the silica network.

The step which controls the overall corrosion rate depends on the glass composition and the environment, particularly pH.

The purpose of this paper is to show that crack growth behavior in some glasses, particularly the binary alkali silicate compositions, can be strongly influenced by alkali ion exchange. The presence of a hitherto undiscovered crack velocity plateau in the 10^{-8} to 10^{-10} m/sec range for these binary glasses will be shown to occur. A model of subcritical crack growth which qualitatively explains the position and slopes of V-K_I curves for different glasses will be discussed.

Table I

Glass	Glass Composition (Mole %)					T_M (°C)	T_A (°C)
	SiO_2	Na_2O	B_2O_5	CaO	MgO		
Soda-lime-silica	*72	14		7	4		
Soda borosilicate	70	7	23			1350	550
33 Na_2O - 67SiO_2	67	33				1350	500
25 Na_2O - 75SiO_2 -	75	25				1400	500

*wt. %

Experimental Procedure

A commercial soda-lime-silica glass and three experimental glasses were investigated. Their compositions are given in Table 1, along with the melting and annealing temperatures for the experimental glasses. The glasses were prepared from reagent grade chemicals melted in a platinum crucible and stirred during firing. Plates were cast on to steel platens and annealed. Double cantilever beam specimens 50 mm x 25mm x 2 mm, were cut from the glass. A groove approximately 1 mm deep was along the center of each specimen to guide the crack. The specimens were then reannealed. Specimens of the two binary soda silica compositions were stored in a dessicator because of the hydroscopic nature of these glasses. Crack propagation tests were run using the double cantilever beam arrangement as described by Wiederhorn.[1] The specimens were dead-weight loaded; the crack position was monitored using a traveling microscope. Stress intensity factors were calculated using Equation 1:

$$K_I = \frac{PL}{(aw)^{1/2}t^{3/2}} (3.467 + 2.315 \ t/L) \tag{1}$$

where P is the load, L the crack length measured from the points of load application, a the web thicknesses, w the total thickness, and t the half width. Tests were run either in an aqueous solution or in air of 22°C and ~30% relative humidity (RH).

The primary solutions used in this investigation consisted of 1 molar Cs^+ and 1 molar Li^+ ions in deionized water. The starting materials were high purity $LiNO_3$ and $CsNO_3$.* The pH of the solutions was varied by the addition of small amounts of HCl or NH_4OH, and monitored throughout the course of the crack growth experiment.

---

*Cerac Co.

Results

Figure 1 shows crack velocity as a function of K_I for soda-lime glass in the 1 M Li^+ and 1 M Cs^+ solutions at three different pH values. Within the scatter of the data, one cannot differentiate between the crack growth behavior in the different solutions. This is not entirely unexpected since Wiederhorn and Johnson[4] found effectively no change in crack growth behavior with changes in buffered solutions of pH 1.8 to 9 for soda-lime glass. One point to note is the apparent crack arrest at a K_I of ∿.27MPam$^{1/2}$ for the soda-lime glass in deionized water. When the apparently stationary crack was reloaded to higher K_I it began to propagate at the velocity expected from the crack growth curves. The change to a steeper slope of the pH 3.5 V-K_I curves at lower velocity is in agreement with the data reported by Wiederhorn and Bolz[2] for crack growth in water at various temperatures. While there is the suggestion of a change to a lower slope in the pH 9 curve, there is not enough data to be definitive.

Borosilicate glass (Figure 2) appears to behave differently when tested in Cs^+ and Li^+ solutions. For any given pH the data taken in Cs^+ solution has the same slope but lies at higher K_I than does the data in Li^+. The pH 7 and 3.5 data overlap while that for pH 9 lies at higher stress intensities. One interesting feature of crack growth in this glass is the crack arrest at K_I ∿ 0.35 MPam$^{1/2}$. The behavior of the cracks upon reloading differed markedly from that in the soda-lime glass; loading the arrested cracks to higher K_I values did not cause them to repropagate. As the cracks were loaded to higher and higher K_I values catastrophic failure finally occurred. Similar behavior was observed by Wiederhorn and Johnson[4] in Pyrex tested in acid environments.

In this borosilicate glass it is impossible to avoid phase-separation during cooling of bulk samples; additional microstructure growth occurs during the anneal at 550°C. The samples tested had an interconnected microstructure (5 - 10 NM) of equal volume fraction of which one phase contains <50% SiO_2. This phase is less resistant to chemical attack than any of the other glasses tested and may account for the severe crack blunting behavior observed only in this glass. Crack blunting is further indicated by the appearance of ridge marks emanating from the position of the stopped crack.[4]

Crack growth data for the 33% soda-silica glass is presented in Fig. 3. Because of the many curves, the individual data points are not shown. There are several important features in this plot. A marked difference between the V-K_I curve measured in air of 30% RH is its location at significantly higher K_I and greater slope compared to those measured in aqueous solutions. The V-K_I data in Cs^+ and Li^+ solutions is clearly separated. In contrast to the borosilicate glass, the data taken in 1M Li^+ lies at higher K_I values than does the Cs^+ data at the same pH, and also has a significantly higher slope. The effects of pH overlap this behavior, with the data for pH 6.5 lying at slightly lower K_I values than either pH 3.5 or pH 9. One significant point is that the data in 1M Cs^+ is identical with that for deionized water. The plateau at low K_I observed in this glass can be seen to be unaffected by the presence of either Cs^+ or Li^+, but the crack velocity at which the plateau growth occurs is dependent on the pH of the solutions, with pH 3.5 lying at higher velocities than pH 6.5. This plateau has been found to extend to K_I's as low as 0.04 MPam$^{1/2}$. Data taken at pH 9 does not show a distinct

plateau; crack velocity continues to decrease with decreasing K_I, but decreases at a much lower rate than in the other portion of the curve.

The crack growth behavior in the 25% soda-silica glass, Figure 4, is quite similar to that in the other binary glass, namely, the data in 30% RH air lies at higher K_I than does the data in the Li^+ and Cs^+ solutions. One interesting feature of the data for this glass is the definite indication of crack arrest in air in direct contrast to the oppositely shaped curves in the Li^+ and Cs^+ solutions. The difference in crack velocity level in solutions with and without 200 ppm of Al^{+3} is related to the dissolution characteristics of this glass as discussed in the next section.

Discussion

It is suggested that the crack growth behavior described previously can be explained by a balance between stress enhanced chemical reactions and the normal corrosion of these glasses in the different solutions. The overall corrosion rate of the glasses studied increases in the order, soda-lime-silica, borosilicate, 25% soda-silica, 33% soda-silica. The soda-lime-silica glass is relatively durable, so a crack growth behavior essentially independent of the exchangeable species in solution, i.e. Li^+ and Cs, and pH between 3.5 to 9.0 is not unexpected.

In the borosilicate glass, the effect of the particular ions in solution is reasonable clear. As noted in the introduction, one step in the glass corrosion process is the exchange of ions in the glass for ions in solutions, i.e., normally H^+. In this case some exchange of Li^+ and Cs^+ ions for Na^+ apparently occurs.

In very non-durable glasses such as the binary soda-silicates, drastic effects of changing the corrosive solution might be expected. In this case Cs^+ seems to produce the same crack growth behavior as water. It is likely that Cs^+-Na^+ and H^+-Na^+ exchange rates are comparable at these solution concentrations and that glasses containing large concentrations of either Cs^+ or H^+ exhibit similar corrosion behavior. Evidence for the latter is the similar corrosion rates measured by infrared reflection spectroscopy for NaO_2-SiO_2 glasses in either 1M Cs^+ solutions or deionized water.[6] In Li^+ solutions the opposite is true; lithia-silica glasses are more durable than soda-silica glass,[6] so that any exchange of Li^+ for Na^+ tends to produce a protective layer which would retard the rate of crack growth. It is hypothesized that the small changes seen in the curves with variations in pH may reflect variations in the degree of hydration of Cs^+ and Li^+ and therefore reflect their ability to exchange with the Na^+ ions in the glass. One possibility which cannot be ignored but which will not be dealt with in this paper is that ion exchange of H^+ for Na^+ produces stresses at the crack tip which influence the growth behavior. Evidence for this is the higher plateau velocity at lower pH plus the observation of small cracks in the bulk glass at pH-1. It was also observed that some peeling of specimen surfaces occurred after drying.

When K_I is lowered to the point where the rate of stress-aided-dissolution equals the normal rate of corrosion, a change in crack tip radius would be expected, as predicted from the theory of Charles and Hillig.[7] In the soda-lime-silica and especially the borosilicate glass, this change in crack tip radius leads to crack arrest. A different phenomenon occurs in the soda silica glasses, namely the crack continues to grow at a velocity which approximates the rate of silica dissolution

in these glasses. The latter hypothesis is based on rates of silica dissolution calculated from the work of Douglas and El Shamy[5] who measured silica extraction rates which would correspond to removal of silica layers in the range of 10^{-9}-10^{-8} m/sec. The saturation of the solution at the crack tip with silica at pH 9 may explain the absence of an observable plateau under these conditions. However, a question arises as to why these cracks continue to grow rather than round out and stop. It is speculated that growth continues because the surface that forms, either as a result of dealkilization and/or reprecipitation of dissolved material, is mechanically weak and relatively nonadherent. It is proposed that even a small stress at the crack tip produces a break in the corrosion layer allowing fresh solution to reach the unreacted glass. The small stress aids removal of material at the tip in preference to removal at other points on the crack surface, so that complete blunting does not occur.

If crack growth rates in this plateau are governed by the rate of stress assisted silica dissolution, one would expect that changes in the solutions which lead to changes in corrosion rates, would be mirrored in changes in this crack growth plateau. Dilmore, Clark and Hench[8] showed that the addition of 200 ppm of Al^{+3} ions to the solution lowers the silica dissolution rate in a binary lithia-silica glass by about an order of magnitude. As shown in Fig. 4 for the 25% soda silica glass, the addition of 200 ppm Al^{+3} also lowers the crack velocity plateau in distilled H_2O by an order of magnitude, giving further credence to the idea of this plateau being strongly influenced by the SiO_2 dissolution rate. One point which is unclear is why the 25% and 33% Na_2O glasses have plateaus in the same range, when their SiO_2 dissolution rates should be quite different. One possibility is that the solution at the crack tip becomes

saturated with SiO_2 and, therefore, stress assisted dissolution cannot occur faster than the SiO_2 diffusion rate away from the crack tip.

This concept of a change from stress-corrosion controlled crack growth to one involving mainly dissolution implies that the crack shape should also change. If the crack shape changes in going from region I to the low level plateau or vice-versa, one should be able to detect the rounding or sharpening of the crack with time. In order to check this, an experiment was conducted in which a crack in the 25% soda silica glass immersed in a 1M Li^+ solution with 200 ppm Al^{+3} (pH=6.5) was allowed to reach a steady state velocity of $\sim 10^{-9}$ m/sec. at a K_I of 0.15 $MPam^{1/2}$. The stress intensity was abruptly raised to 0.50$MPam^{1/2}$, at which point the steady state crack velocity should have been $\sim 10^{-5}$ m/sec. Even though an initial sharp increase in V occurred, (Fig. 5), the crack velocity reached the expected value only after approximately 1 hour under load, after which time the velocity remained constant. The measurement of the initial jump could be in considerable error because of the small amount of crack extension that occurred. This data suggests that a gradual reduction in crack tip radius was required (the balance between corrosion and stress corrosion had to be readjusted) before a steady state velocity could be reached at the higher K_I.

Variations in crack tip shape are postulated to occur throughout the regime of subcritical crack growth. From the data for region I crack growth (Fig. 6) one can see a significant difference between the slopes and positions of the different curves depending on the glass composition and test environment. If one looks in particular at the binary soda-silica glasses, it is apparent that the V-K_1 curves for the less chemically durable 33% soda glass lie at higher K_I values than the 25% soda glass in either Cs^+ or Li^+ solutions. This is opposite to what

one might initially expect from the rates of corrosion. This feature of
the data suggests that crack tip shapes may differ in different glass
compositions and that the less durable glasses have larger crack tip
radii and therefore smaller stress fields (than would be calculated from
fracture mechanics theory) at their tips. One possible model would
suggest that the two primary factors determining the position and slope
of a $V-K_I$ curve are the rate of corrosion, a process which tends to
round the crack tip, reducing the stress intensity, and the stress
dependence of the corrosion process which tends to produce a sharper
crack. This concept is in direct analogy to the model of Charles and
Hillig.[7] We are suggesting that each glass composition has its own
crack tip radius which decreases with increasing stress intensity and
that this decrease in crack tip radius with increasing stress intensity
gives rise to the slope in the $V-K_I$ curves. One anomally to this model
is fused silica, which should have a very low corrosion rate, yet lies
well to the right of any of the crack growth curves shown in Figure 6.
It may be, however, that the type of corrosion product formed may also
have a significant influence on the crack growth behavior so that one
may need to compare families of glasses rather than compare glasses of
widely varying composition. This kind of comparison is suggested by
the work of Hench et. al.[9] who showed that corrosion behavior in glasses
could be of at least 5 different types. Another possible anomally is
the behavior of the soda-silica glasses in air, where their resistance
to stress corrosion seems to be significantly higher, even though one would expect
the crack tip radii to be smaller because of lower corrosion rates.
However, corrosion products may be easily removed in solutions while being
trapped at the crack tip in air, thereby hindering the reactants from

reaching the unreacted material. Secondly, there is a much smaller
concentration of water to react with the surface. Both factors would
lead to reduced stress corrosion rates.

Summary and Conclusions

Crack velocities have been measured as a function of K_I for four
different glasses in solutions of Li^+ and Cs^+ held at different pH. The
data for soda borosilicate and the two binary soda-silica, glasses show
definite effects of the presence of Li^+ or Cs^+ ions. In the binary
glasses, the $V-K_I$ curves in Li^+ lie at higher K_I's because of the formation
of a protective layer, and are steeper than those obtained in either Cs^+
or deionized water because the ion exchange rate of Li^+ for Na^+ is slow
enough so that as the crack velocity increases, the concentration of Li^+
in the surface is steadily reduced until the protective layer no longer
forms. In the case of Cs^+ and H^+, ion exchange rates are higher and so
can keep up with crack growth rates over a much larger range of velocities.
Changes in pH are shown to produce smaller shifts in these curves.

A plateau in crack velocity is observed for the binary glasses at
$0.04 < K_I < 0.35$ MPam$^{1/2}$. The value of the velocity plateau appears to
depend on the SiO_2 dissolution rates of the glass in the given solution,
but some affect of local stresses due to ion exchange cannot be ignored.

It is concluded from crack acceleration experiments that changes in
crack tip shape must take place as a crack propagates from the low level
plateau into Region I. A model of environmentally assisted crack growth
is put forth which suggests that the position and slope of the $V-K_I$
curve for a particular glass in a given environment is governed by a
balance between the tendency of corrosion processes to increase the
crack tip radius and the stress corrosion process which would sharpen
it.

Acknowledgements

References

1. S.M. Wiederhorn, "Influence of Water Vapor on Crack Propagation in Soda-Lime Glass," J. Am. Ceram. Soc., 50 [8] 407-414 (1967).

2. S.M. Wiederhorn and L.H. Bolz, "Stress Corrosion and Static Fatigue of Glass", J. Am. Ceram. Soc. 53, [10], 543-548 (1973).

3. S.W. Freiman, "Effect of Alcohols on Crack Propagation in Glass," J. Am. Ceram. Soc., 57 [8] 350-53 (1974).

4. S.M. Wiederhorn and H. Johnson, "Effect of Electrolyte pH on Crack Propagation in Glass," J. Am. Ceram. Soc., 56, [4] 192-97 (1973).

5. R.W. Douglas and T.M. M. El-Shany, "Reactions of Glasses with Aqueous Solutions", J. Am. Ceram. Soc., 50 [1], 1-8 (1967).

6. C.J. Simmons, S.W. Freiman and L.L. Hench, "Comparison of Corrosion and Stress Corrosion Rates in Alkali-Silicate Glasses", Bull. Am. Ceram. Soc. 59, 865, (1980).

7. W. B. Hillig and R.J. Charles, pp 682-705 in High Strength Materials., Eidted by V. F. Zackey, John Wiley & Sons, Inc., New York, 1965.

8. M.F. Dilmore, D.E. Clark, and L.L. Hench, "Corrosion Behavior of Lithia Disilicate Glass in Aqueous Solutions of Aluminum Compounds," Bull. Am. Ceram. Soc., 58 [11] 1111-17 (1979).

9. L.L. Hench, "Physical Chemistry of Glass Surfaces", Proceedings of the XIth Congress on Glass, Prague, 1977.

Figure Captions

Figure 1 - Crack Velocity - K_I plots for soda lime silica glass tested in 1M Li^+ and 1M Cs^+ solutions, and deionized water. Note apparent cracks arrest at K_I = 0.27 MPam$^{1/2}$ slope of the line through the data $\simeq$ 19.
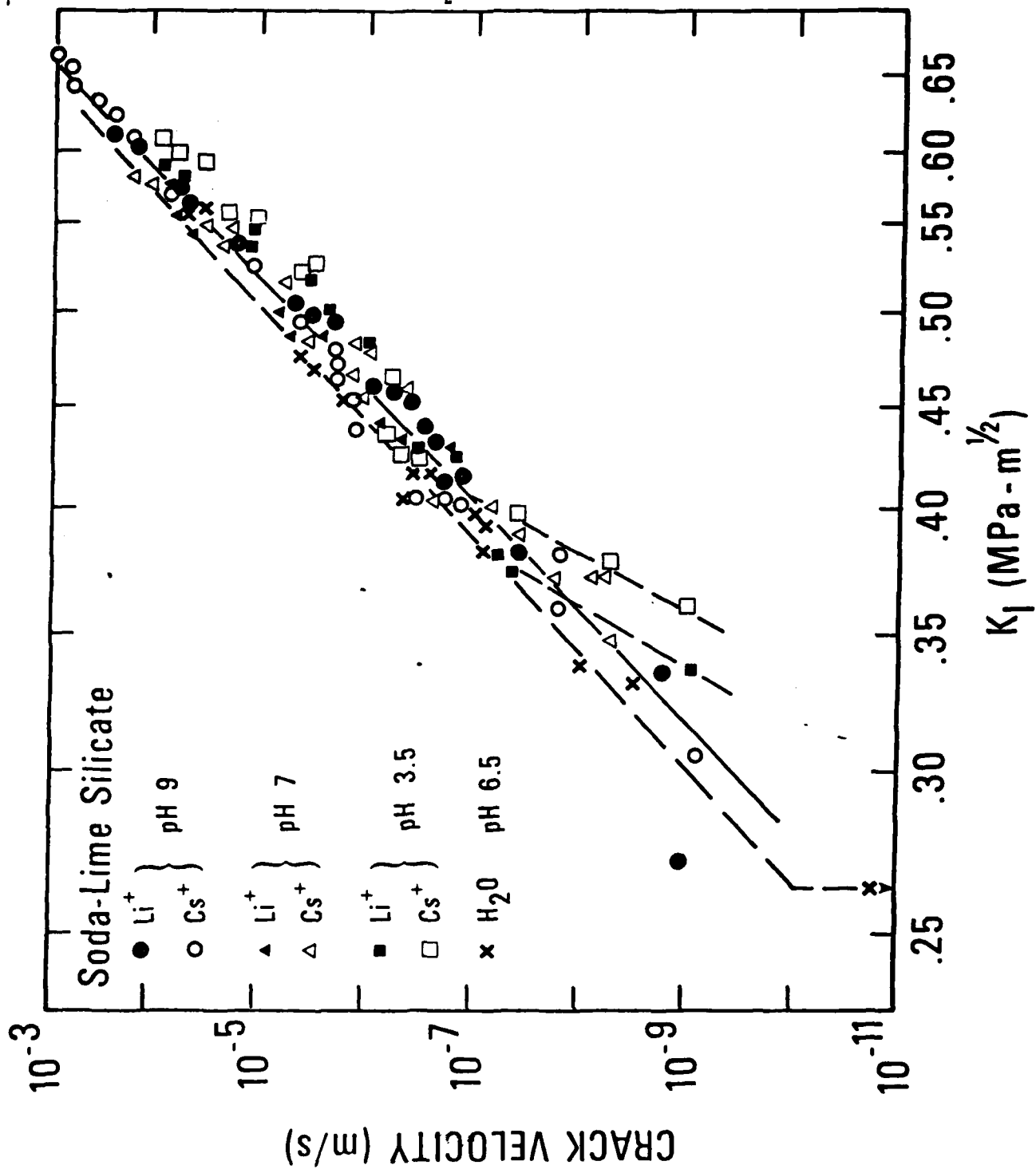
Figure 2. Crack velocity - K_I plots for soda borosilicate glass tested in the same solutions as in Figure 1. Note the definite separation in the curves for Cs^+ and Li^+, with the former lying at higher K_I's than the latter for all pH ranges investigated. The slope of all the curves is $\simeq$ 35.
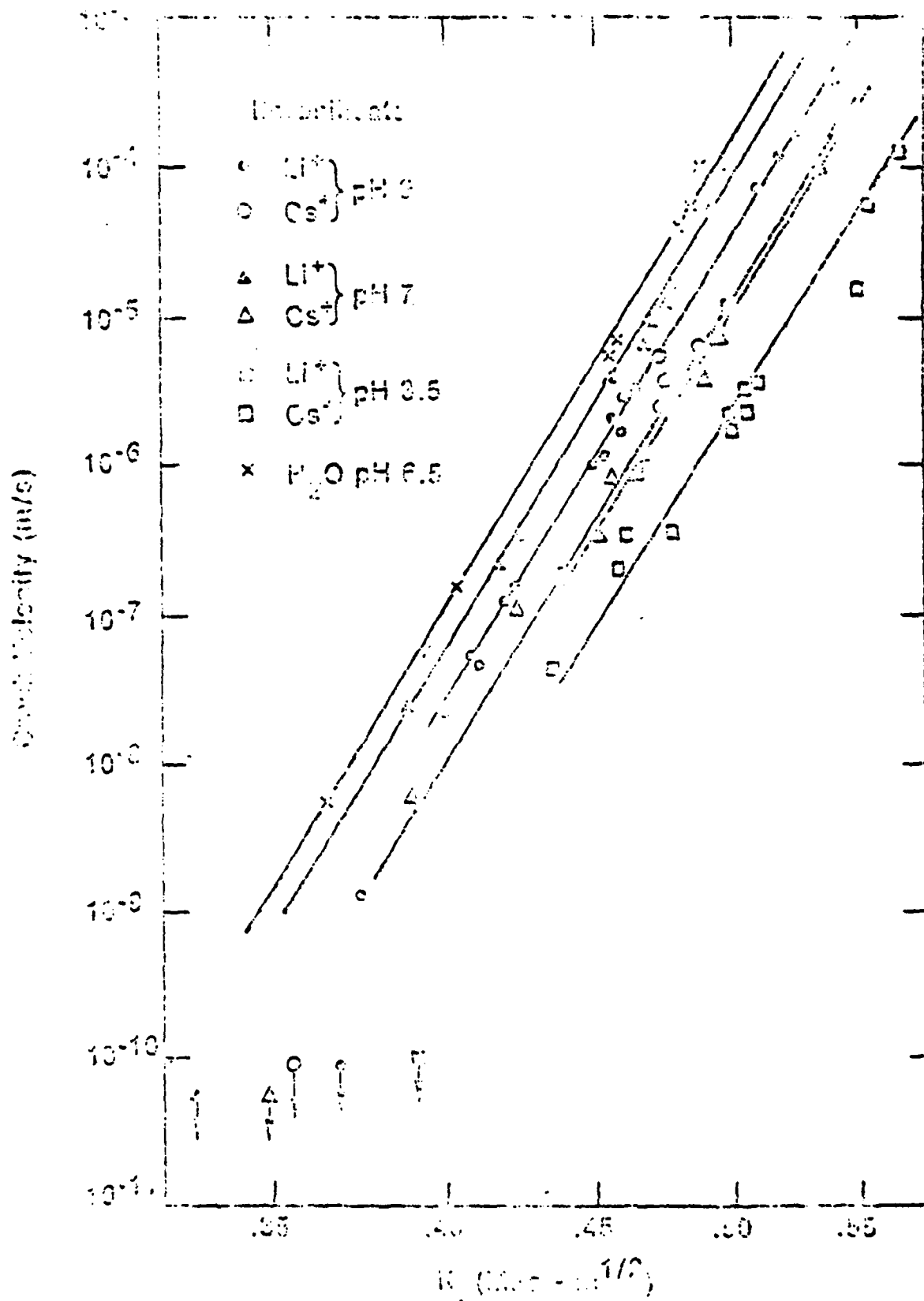
Figure 3. Crack velocity-K_I plots for 33% Na_2O-SiO_2 glass in the different environments. Note that curves in Li^+ are steeper and higher K_I than those in Cs^+. The data taken in deionized water overlaps that in Cs^+.

Figure 4. Crack velocity -K_I plots for 25% Na_2O-SiO_2 glass in different environments. Note that data obtained in any solution containing $\sim$200 ppm Al^+ lies on the lower of the two plateaus. A definite crack arrest was observed in this glass tested in air.

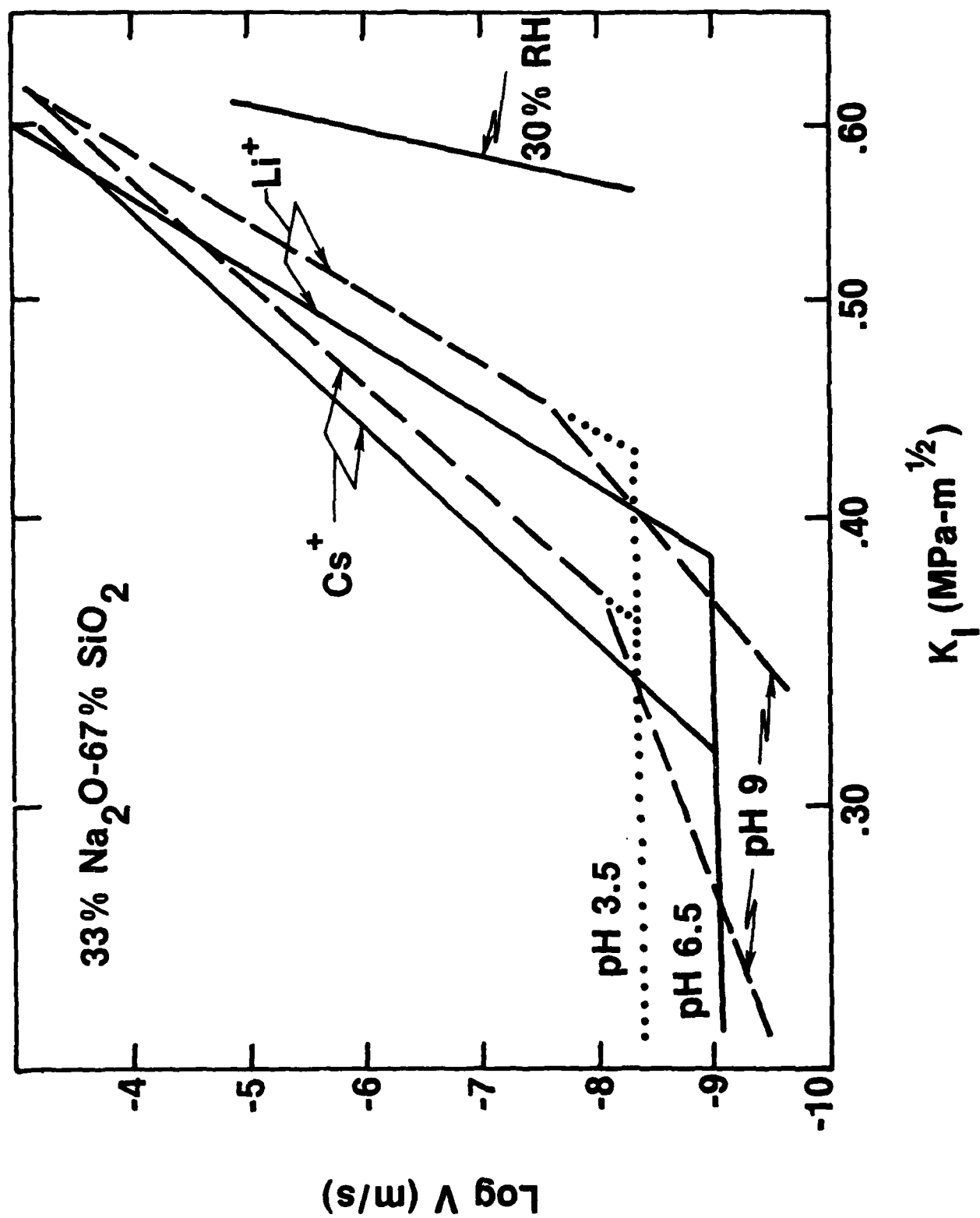Figure 5. Crack velocity in 25% Na_2O-SiO_2 glass as a function of time at a stress intensity of 0.53 MPam$^{1/2}$. Crack was initially propagating at a velocity of $\sim$10^{-9} m/sec. when K_I was raised.

Figure 6. Comparison of V-K_I curves in Region I for all glasses investigated in this study.

Soda-Lime Silicate

	Li$^+$	Cs$^+$	
●	○	} pH 9	
▲	△	} pH 7	
■	□	} pH 3.5	
✕	H$_2$O	pH 6.5	

CRACK VELOCITY (m/s)

K_I (MPa-m$^{1/2}$)

33% Na$_2$O-67% SiO$_2$

25% Na$_2$O - 75% SiO$_2$
1M Li$^+$ Solution at pH 6.5

$$\left[\begin{array}{l} V = 3.5 \times 10^{-5} \text{ m/s} \\ K_I = 0.5 \text{ MPa m}^{\frac{1}{2}} \end{array} \right]$$

Measured Velocity/Expected Velocity (y-axis)

Time At Constant Load (min) (x-axis)

- 32 -
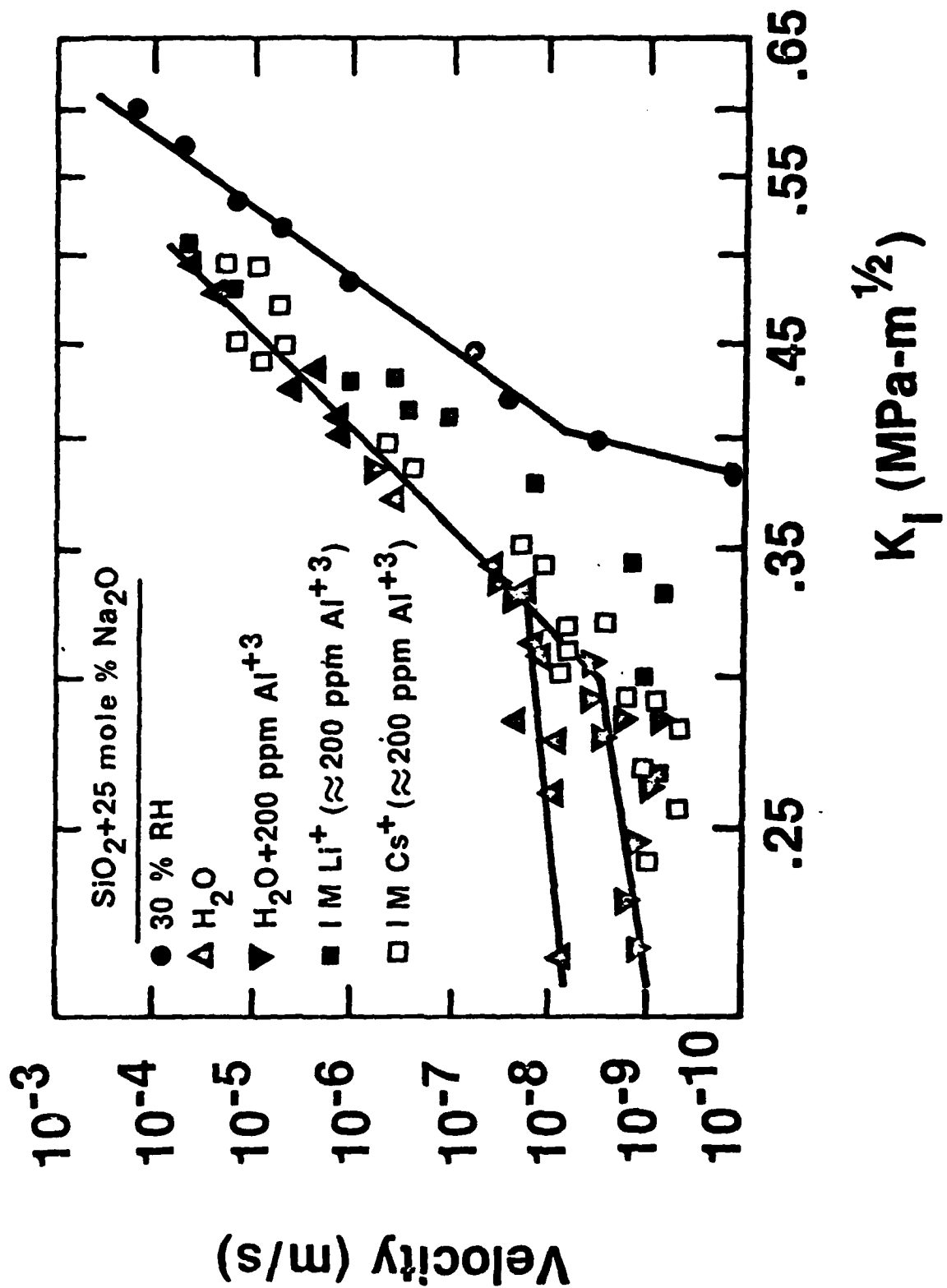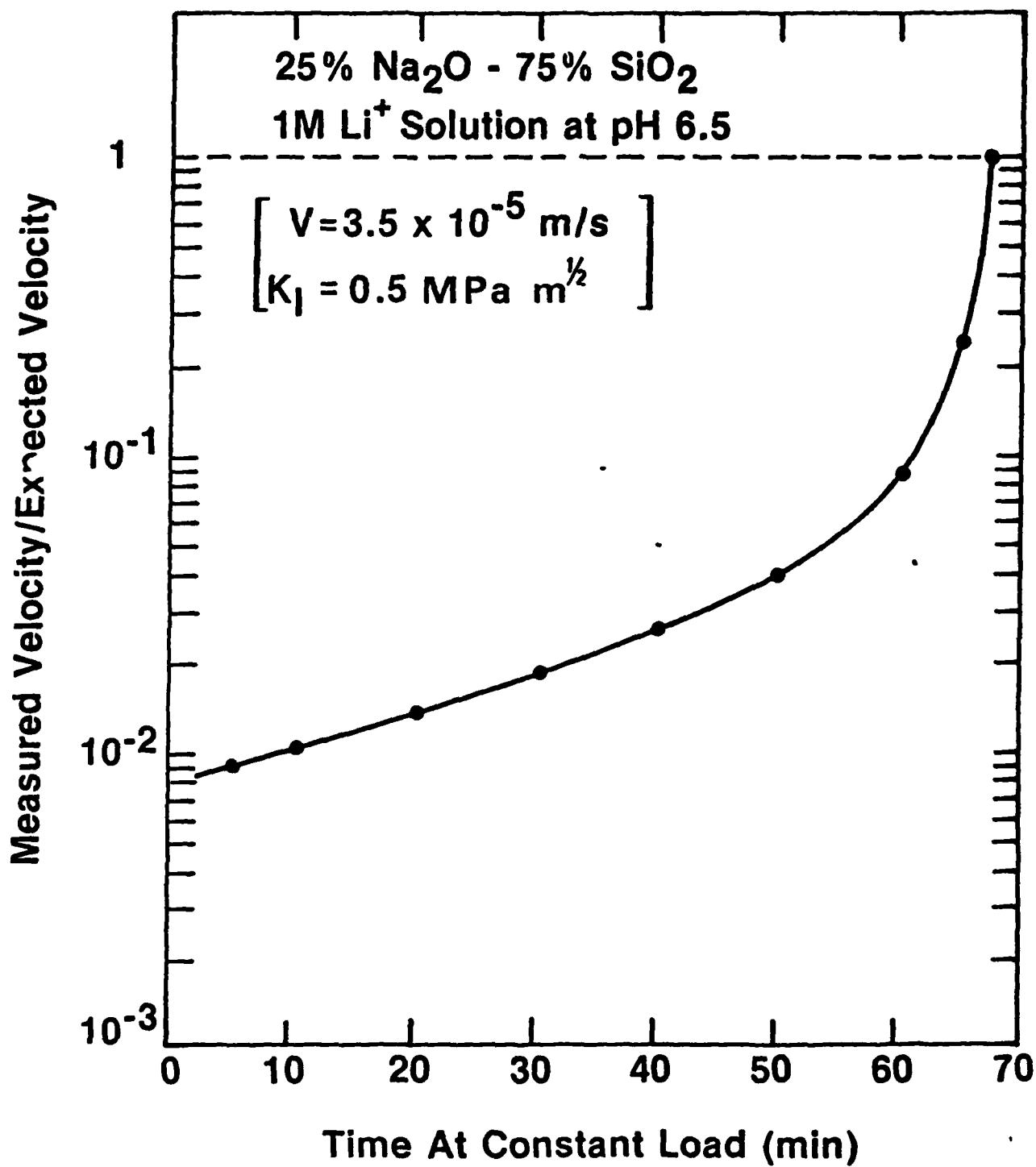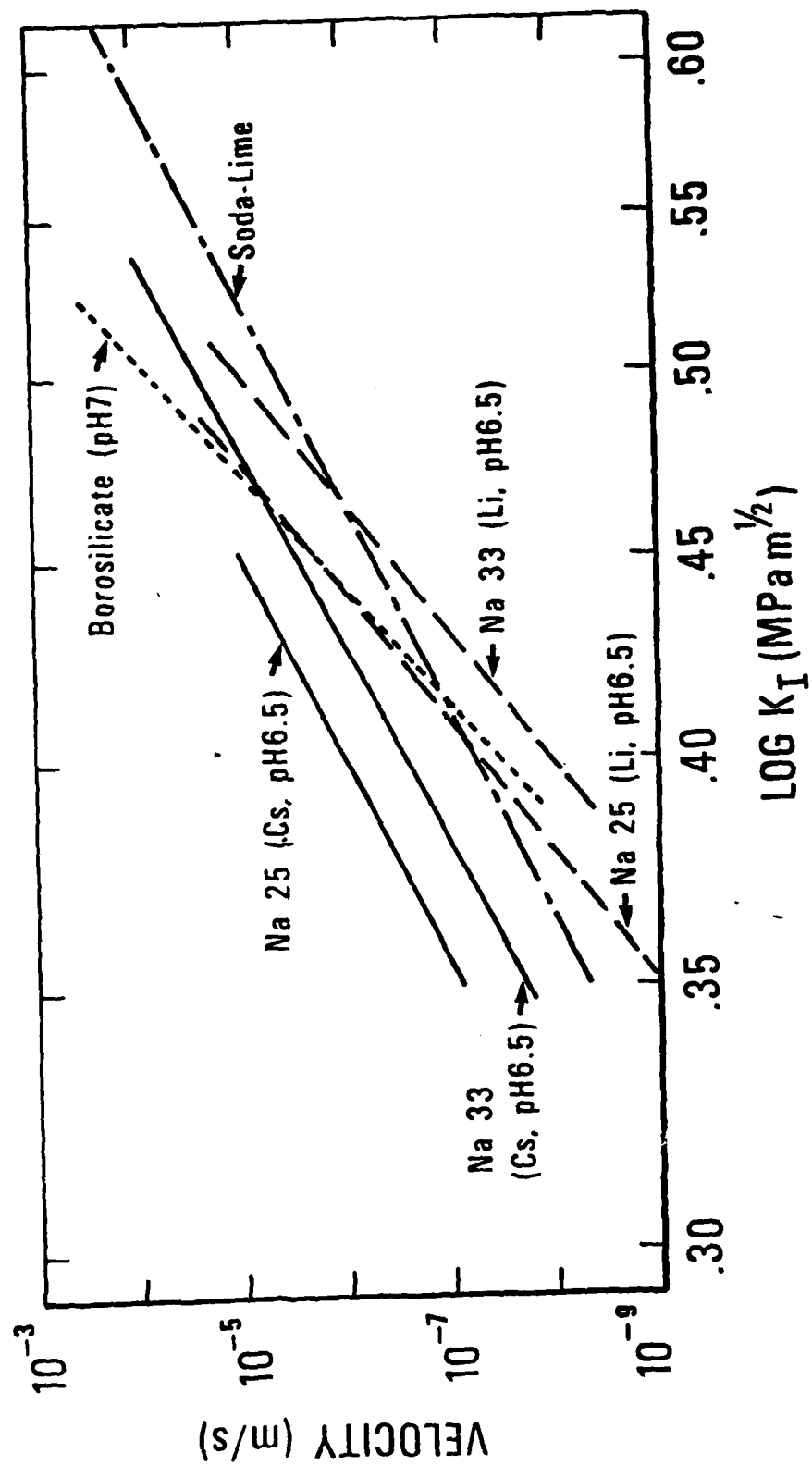
Raman investigation of optical fibers under high tensile stress [a]

G. E. Walrafen

Department of Chemistry, Howard University, Washington, D. C. 20059

P. N. Krishnan

Department of Chemistry, Coppin State College, Baltimore, Maryland 21216

S. W. Freiman

National Bureau of Standards, Gaithersburg, Maryland 20234

Raman spectra have been obtained from fused silica optical fibers under tensile stresses from 0 to 3.3 GPa (33 kbars). Reversible intensity *increases*, relative to the principal Raman maximum at 440 cm^{-1}, were observed for the defect peak at 490 cm^{-1} and for shoulders near 350–375 and 115 cm^{-1}. Application of tensile stress to fused silica appears to produce changes in the stretched Si—O defect sites, as well as changes in the main network structure.

PACS numbers: 63.50. + x, 78.30.Jw, 81.20.Pe

INTRODUCTION

Raman features from fused silica near 490 and 604 cm^{-1} have been examined in several recent investigations,[1-7] see Fig. 1 (stars). Raman intensities at 490 and 604 cm^{-1} were found to increase with increasing fictive temperature T_F when the OH content was constant (or zero).[4] The 490- and 604-cm^{-1} Raman intensities were also observed to decrease with increasing OH content at constant T_F.[4] In the latter case a weak Raman band near 970 cm^{-1}, due to Si versus OH stretching,[4,8] was produced at the expense of in-

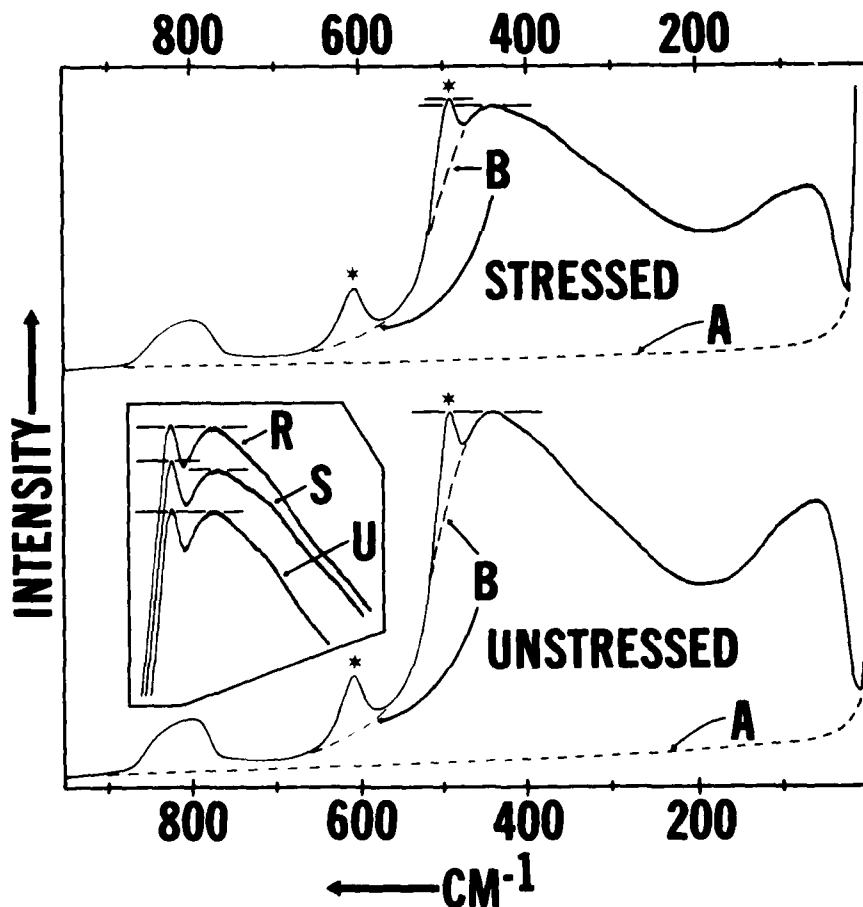FIG. 1. Forward Raman scattering from fused silica optical fiber stressed to 3.34 GPa (upper), and unstressed (lower). Spectra in the inset were obtained in the sequence unstressed U; stressed S to 2.19 GPa; and relaxed R. Note that the inset spectra have been moved to the left—their position does not correspond to the cm^{-1} values below them. Baselines A and B are shown by dashes.

- 33 -

tensity at the 490- and 604-cm^{-1} positions. Other findings, such as the observation that the 490- and 604-cm^{-1} intensities from samples having high T_F's could be reduced by annealing, strengthened the hypothesis that these peaks could be assigned to defects in the silica structure.[4]

The nature of the above defects suggested that their concentration and/or molar intensity should increase under the application of tensile stress. In order to subject a sufficient volume of glass to large tensile stresses,[9] experiments were conducted on glass optical fibers. An interpretation of the changes observed in the Raman spectrum is presented in terms of variations in the Si—O binding at defect sites.

EXPERIMENTAL PROCEDURES

Pure fused silica optical fibers were used in all experiments (silicone rubber cladding, 200 μm diameter).[10] The OH content of the fibers was about 530 ppm,[11] and T_F values were estimated to be roughly 1700–1800 °C.[12] The constancy of the OH concentration was assured by monitoring the Raman OH-stretching intensity near 3700 cm^{-1}.[13]

Forward scattered Raman spectra were obtained by focusing the fiber output on the entrance slit of an Instruments S. A. HG2S holographic grating double monochromator (Fig. 2). Raman excitation was accomplished using 514.5-nm argon ion laser radiation at about 0.6 W. Slit widths ranged from 2 to 3 cm^{-1}, and detection was accomplished with an uncooled Hamamatsu R928 PM tube, a Keithley 414S picoammeter, and a high-speed Esterline Angus L1101S recorder.

Load was applied to the fiber by suspending a weight from a clamp near the end of the fiber (Fig. 2). The optical fiber was held by strips of sponge rubber placed between wooden strips 30–50 cm in length, tightly clamped together in several places. This arrangement prevented any slippage during application of load. The stressed-to-unstressed length ratio was maintained in the range of 5–50 to reduce the unstressed spectral contribution.

Some Raman experiments were also attempted in which only stressed fiber was examined by focusing 90° scattered radiation on the slit, but these experiments were abandoned because the S/N (signal-to-noise) ratio, although good, was at least 20-fold lower than that obtained from forward Raman scattering.

Because the Raman depolarization ratio varies across the fused silica spectrum,[14] it was necessary to determine if the polarization, which is ordinarily scrambled by an optical fiber, changes under tensile stress. Preliminary experiments involved examination of the mode structure and the polarization at the fiber output. No significant changes were observed in the high-order mode structure under stress, and no changes whatever in polarization were detected using polarizers or crossed polarizers.

Quantitative measurements of the polarization were made using the optical fiber emission to excite both forward and 90° Raman scattering in liquid CCl$_4$. Ratios of integrated Raman intensities were determined for the CCl$_4$ peaks at 218(dp), 314(dp), and 459(p) cm^{-1}. (Here dp refers to a depolarization ratio of 0.75 and p to a ratio of about 0.01.[15] For
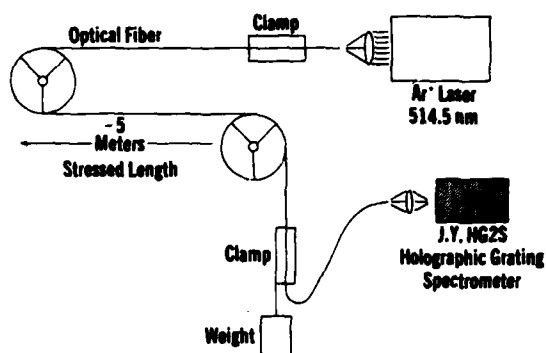

FIG. 2. Schematic illustration of method used to obtain forward Raman spectra from an optical fiber while applying tensile stress.

both forward and 90° scattering, no changes whatever were detected in the intensity ratios I_{459}/I_{314} and I_{459}/I_{218} for tensile stresses to 2.19 GPa. Further, the intensity ratios obtained from CCl$_4$ were those characteristic of unpolarized excitation, as expected from the fact that polarization is scrambled by internal reflection in high-mode optical fibers. Also, it should be emphasized that the above integrated Raman intensity ratios from CCl$_4$ constitute a particularly sensitive test of the polarization properties of the exciting radiation emitted from the optical fiber.

RESULTS

Stressed and unstressed Raman spectra illustrative of the approximately 50 individual experiments performed are shown in Fig. 1. The (upper) spectrum was taken at a tensile stress of 3.34 GPa (33.4 kbars), while the lower spectrum was taken from an unstressed fiber. The intensification of the 490-cm^{-1} defect peak (starred), relative to the 440-cm^{-1} peak, is visually obvious, and is emphasized by the horizontal lines. In the unstressed spectrum, the 490- and 440-cm^{-1} peaks occur at the same vertical height as seen by the horizontal line through them, but at 3.34 GPa (upper) the 490-cm^{-1} peak height is well above the horizontal line. Similar conclusions may be drawn from examination of the inset of Fig. 1 which refers to three spectra run in the sequence unstressed U; stressed S at 2.19 GPa, S and relaxed R with 20–30 min between spectra.[16]

The visual observation that the 490-cm^{-1} peak height increases relative to the 440-cm^{-1} peak height, i.e., that I_{490}/I_{440} increases, may mean either that I_{490} increased at constant I_{440}, or that I_{440} decreased at constant I_{490}, or that both I_{490} and I_{440} changed, or even that more complicated changes occurred, such as broadening, etc. Hence, if I_{440} is to be regarded as a reference standard, it is desirable to understand how I_{440} varies relative to other peaks, such as the intense peak at 60 cm^{-1}.

Peak heights above baseline A in Fig. 1, were measured for the 60-, 440- and 800-cm^{-1} peaks at a series of tensile stresses. Consistency of drawing baseline A under all spectra was obtained by using a single template whose shape, baseline A in Fig. 1, was determined through repeated trials. The

2833   J. Appl. Phys., Vol. 52, No. 4, April 1981   Walrafen, Krishnan, and Freiman   2833

- 34 -

template was positioned to a given Raman spectrum by simultaneously matching two regions: (1) the region between the exciting line and the sharp minimum near 20 to 25 cm^{-1} and (2) the region from about 900–1000 cm^{-1}. The results are shown in Table I in terms of the ratios I_{60}/I_{440}, I_{800}/I_{440}, and I_{800}/I_{60}.

The average value for the peak height ratio I_{60}/I_{440} from Table I is 0.70 $\pm$ 0.02, which within present errors is constant. Similarly, the ratios I_{800}/I_{440} and I_{800}/I_{60} are also seen to be constant (Table I). The constancy of the ratio I_{60}/I_{440} is particularly important because the peaks at 60 and 440 cm^{-1} have both the largest peak heights and the highest integrated intensities (Fig. 1) in the fused silica spectrum.

Quantitative values of peak height ratios are often difficult to obtain accurately when weak features such as at 490 and 604 cm^{-1} are involved because such ratios suffer from errors in baseline estimates and peak S/N ratios. Peak height ratios also ignore component broadening. A better method is to use ratios of integrated intensities. For the 490- and 604-cm^{-1} peaks (Fig. 1), integrated intensities may be obtained using baseline B. Baseline B was obtained by using a French curve. In contrast, an integrated intensity for the 440-cm^{-1} component could not be readily obtained because the component shape is unknown. Therefore the total integrated Raman intensity from about 20 to 900 cm^{-1} was obtained using baseline A minus, of course, the contributions from the 490- and 604-cm^{-1} components. The resulting ratios of integrated Raman intensities I_{490}/I_T and I_{604}/I_T, where T refers to the total Raman area minus the 490- and 604-cm^{-1} component areas, are shown for tensile stresses from 0 to 2.19 GPa in Table II. In addition, the quantities I_{490}/I_{440} and I_{604}/I_{440} are listed in Table II, where I_{490} and I_{604} are integrated intensities above baseline B, and I_{440} refers to the peak height above baseline A. The latter ratios were used in Table II because of the intensification of shoulders described subsequently. It should also be made very clear that the 490-cm^{-1} component area (the integrated component intensity) obtained above baseline B is independent of effects due to broadening of the 440-cm^{-1} component. Slight broadening of the 440-cm^{-1} component was clearly evident from changes in the shape of baseline B under the 490-cm^{-1} peak, but this broadening effect was completely negated by use of baseline B.

It is apparent from Table II that the only significant changes involve the 490-cm^{-1} component, as previously

TABLE I. Raman peak height ratios (I refers to peak height) for the 60-, 440-, and 800-cm^{-1} peaks from fused silica for tensile stresses to 2.19 GPa.

Stress (GPa)	I_{60}/I_{440}	I_{800}/I_{440}	I_{800}/I_{60}
0	0.68	0.17	0.25
0.31	0.69	0.17	0.24
0.62	0.69	0.17	0.25
0.94	0.71	0.17	0.24
1.25	0.72	0.17	0.24
1.56	0.71	0.18	0.25
1.87	0.67	0.17	0.26
2.19	0.71	0.18	0.25

TABLE II. Ratios of integrated Raman intensities and peak heights for the 440-, 490-, and 604-cm^{-1} peaks from fused silica. I_{490} and I_{604} refer to integrated component intensities above baseline B (Fig. 1). I_T is the total integrated intensity above baseline A minus the 490- and 604-cm^{-1} component areas above baseline B. I_{440} is the peak height above baseline A at 440 cm^{-1}.

Stress (GPa)	I_{490}/I_T	I_{604}/I_T	I_{490}/I_{440}	I_{604}/I_{440}
0	0.011	0.013	0.0009	0.0011
0.31	0.011	0.015	0.0009	0.0012
0.62	0.012	0.014	0.0010	0.0011
0.94	0.014	0.013	0.0011	0.0011
1.25	0.016	0.013	0.0013	0.0011
1.56	0.016	0.015	0.0013	0.0012
1.87	0.016	0.013	0.0013	0.0011
2.19	0.017	0.013	0.0015	0.0011

suggested from examination of Fig. 1. The original data leading to Table II (using three figures, instead of the two significant figures of Table II) were treated by linear least squares. Changes of about 62% in I_{490}/I_T, and of about 67% in I_{490}/I_{440}, resulted for stresses to 2.19 GPa, using the least-squares estimates, but changes in the ratios involving the 604-cm^{-1} component were not significant (negligible). Because the relative 604-cm^{-1} intensity did not change with tensile stress, it can be concluded from Tables I and II that Raman intensities at 60, 440, 604, and 800 cm^{-1} are either all independent of, or vary in the same way with, tensile stress.

In addition to relative intensification of the 490-cm^{-1} peak, other small spectral changes were seen for Raman features below 440 cm^{-1}. One effect which occurred consistently throughout this work is an apparent enhancement under tensile stress of a shoulder near 350–375 cm^{-1}, evident from careful examination of Fig. 1, particularly the inset. In the inset, the region from about 440 to 350 cm^{-1} has the same slope in both the U and R spectra. However, this slope is smaller for the S spectrum, indicating a slight intensification of the 350–375 cm^{-1} shoulder component. However, the 350–375 cm^{-1} shoulder would also appear to intensify if the 440-cm^{-1} component broadened. Experience with baseline B at high tensile stress indicates a slight but definite broadening of the 440-cm^{-1} component, which could account for part (or all) of the intensification at 350–375 cm^{-1}. In regard to intensification due to broadening of neighboring components, it should be emphasized again that the relative intensification at 490 cm^{-1} *cannot* be so explained because the 440-cm^{-1} broadening is subtracted from the integrated intensity at 490 cm^{-1} by virtue of curvature in baseline B (Table II).

Some shape changes may also occur in the Raman region between 0 and 200 cm^{-1} under increasing tensile stress. A shoulder at roughly 115 $\pm$ 5 cm^{-1} appears to be more prominent under high stress, compared to the nominal 60-cm^{-1} intensity maximum (Fig. 1). The Raman amplitude ratio I_{115}/I_{60}, using the method A baseline, increases roughly 5% in the figure. The position of the Raman peak at 60 cm^{-1} seemed not to rise in position significantly, however. For tensile stresses from 0 to 2.19 GPa, the position ranged from

- 35 -

60 ± 2 to 63 ± 2 cm^{-1}, i.e., about constant. However, it was not possible to determine whether or not the relative intensification at 115 cm^{-1} resulted from an increasing half-width of the 60-cm^{-1} component.

DISCUSSION

Three distinct types of behavior have now been delineated in regard to the intensity variations of the 490- and 604-cm^{-1} peaks from fused silica as follows: (1) Intensity increases at *both* the 490- and 604-cm^{-1} positions with increasing T_F,[4] (2) a large intensity increase at 604 cm^{-1} relative to the 490-cm^{-1} peak observed when fused silica is densified by neutron irradiation,[2] and (3) the reversible Raman intensity increase at 490 cm^{-1} *observed here. It should be emphasized, however, that the type 1 and 2 variations differ markedly from the type 3 variation*—annealing is required to produce reversibility for types 1 and 2.

In previous Raman work[2-4] lines near 490 and 604 cm^{-1} were assigned to defects of the type —Si—O···Si—, where the dots refer to a broken bond. However, in view of the electron paramagnetic resonance inactivity of ordinary bulk fused silica,[17] it is more appropriate to think of the defect as a stretched bond, or related to the effects of a stretched bond. Such a stretched bond would have a smaller force constant, i.e., would be dynamically weakened but would certainly not be broken from an energetic point of view, that is, it would not be a point defect in the usual sense. Such a "defect" could be considered as a Si—O bond associated with a small (e.g., less than 120°) bridging bond angle, and consequently with a large (e.g., greater than 1.68 Å) Si—O bond length.[18]

In regard to a decreased force constant, no significant frequency shifts were observed in this work and in previous Raman work[4] for the defect lines at 490 and 604 cm^{-1}. Also the shifts reported for the defect lines by Bates *et al.*[2] are 2% or less. Thus, the 490- and 604-cm^{-1} lines probably refer to vibrational modes affected by, *but not directly related to*, the Si—O elongation involved. Further, the 490- and 604-cm^{-1} Raman lines are unusually sharp for glasses. Thus, it is not unreasonable to relate these lines to local modes decoupled from the silica network by virtue of the stretched Si—O bond, e.g., modes of the O_3Si or $OSiO_3$ units and/or of the O_3Si—$OSiO_3$ grouping, in which one intervening and elongated Si—O bond replaces the dots in the previous —Si—O···Si— picture. Because the concentration of stretched Si—O bonds may be only about 6×10^{19}/cm^3,[4,19] or about 0.1%, a significant lowering of the stretching frequency at 1060 cm^{-1} would not be expected, that is, most of the Si—O vibrations correspond to the main glass structure.

In previous Raman studies of fused silica, it was estimated that a small fraction, roughly 6×10^{19}/cm^3 of defects,[4] for example, of highly elongated Si—O bonds might exist. This high-energy fraction would be "frozen" into the thermodynamically unstable structure that is produced by rapid quenching. Because such elongated bonds would constitute high-energy sites, they would probably react preferentially with water to form adjacent Si—OH groups.[13] Further, high tensile stress might also increase the fraction of

elongated Si—O bonds. Or, high tensile stress could alter structures immediately associated with the elongated bonds, i.e., the effects of temperature rise and of tensile stress could be very different mechanistically. At any rate, the defects envisioned here are topological network defects associated with elongated high-energy Si—O bonds whose concentrations may be changed by changes in T_F, or alternatively through preferential chemical reaction with H_2O (Refs. 3 and 4), GeO_2, or B_2O_3,[3] etc.

It should also be mentioned that when uniaxial stress is applied to fused silica, changes such as the intensification of Raman shoulders at $350-375$ cm^{-1} and at 115 ± 5 cm^{-1} occur, along with the intensity increases at 490 cm^{-1}. Apparently, the main silica network suffers reversible distortions, as well as the reversible bond elongations related to the defects. The intensifications of Raman shoulders observed here are significant, and do not appear to have been observed previously.

The magnitude of the intensity changes observed in the tensile stress experiments can be shown to be surprisingly large compared to the energy imparted to the fused silica optical fiber by virtue of the work done in stretching it. Our measurements indicate that a 7-kg weight, when suspended from a fiber 200 μm in diameter (tensile stress, 2.19 GPa) and 447 cm long, stretches the fiber about 12.7 cm. The work done is thus 0.41 kcal/mol SiO_2, or 14.8 cal/cm^3 SiO_2. This work amounts to only 0.2% of the standard heat of formation of SiO_2 glass at 25 °C, $(\Delta H_f^0 = 202.5$ kcal/mol SiO_2),[20] and thus it is 10^{-3} times smaller than the Si—O bond energy. (*The Si—O bond energy may be crudely approximated by dividing the ΔH_f^0 by 4 because there are 4 Si—O bonds per stoichiometric SiO_2.*) However, if the defects involve stretched, rather than broken bonds, and the energy due to stretching goes disproportionately into the defect sites, the effect would be non-negligible. In this regard, the following calculation, although forced, is instructive.

Consider that the defect concentration is roughly 6×10^{19}/cm^3,[4] and that this concentration increases 60–70% due to tensile stress, as might be inferred from the increase in the I_{490}/I_{440} ratio (Table II). Then the change in the defect concentration would be about 4×10^{19}/cm^3. Because there are 4 Si—O bonds per stoichiometric SiO_2, the total concentration of Si—O bonds is about 9×10^{22}/cm^3, which means that the fraction changed by stretching would be 4×10^{-4}. The product of the work, about 15 cal/cm^3, times 4×10^{-4} is 0.01 cal/cm^3, which would be the energy imparted by equipartition to the new defects contained in 1 cm^3. Because this amount of energy seems negligibly small, and the Raman intensity change at 490 cm^{-1} is visually obvious, a disporportionate amount of the work of stretching might go into creating new defects. The remaining energy, which certainly is most of the work of stretching, would go into the main silica network, as evidence by shape changes near 350–375 and 115 cm^{-1}. Alternatively, because T_F is constant during stretching, a small fraction of the work of stretching could go into stretching the existing temperature-induced defects even farther, as opposed to creating new defects. This additional stretching could produce structural changes

- 36 -

which result in matrix element effects leading to increased intensity at 490 cm^{-1}. Unfortunately, this alternative process, although almost certainly more realistic than one involving production of additional new defects, is virtually impossible to approximate energetically at this time.

With regard to mechanistic differences between fictive temperature and uniaxial tensile stress, the reversible nature of the present experiments should be strongly emphasized. For example, annealing is required to remove the neutron-induced defects which give rise to greatly increased Raman intensity at 604 cm^{-1}.[2] Whereas, with application of tensile stress, the Raman spectral changes are reversible within 20–30 min,[16] (although the actual relaxation times, which are probably very short compared to 20 min, have not been measured[16]). Further, the present relaxational behavior may also be contrasted to the situation in which qualitatively similar Raman intensity changes in the 490- and 604-cm^{-1} defect components resulted for samples having T_F values of 1400 °C, after annealing for 200 h at 1100 °C.[4] Hence, the presently observed reversibility is in accord with a bond stretching mechanism, whereas bond breaking or the production of new defects would probably be irreversible at room temperature.

Since completion of this work, Raman experiments have been conducted of the rate of increase of the OH-stretching peak intensity at 3700 cm^{-1}, relative to the 800-cm^{-1} silica peak intensity, for a silicone rubber clad fused silica optical fiber, with and without tensile stress. To stresses of 1.56 GPa, *no significant increase* in the rate of the OH-stretching intensity, *above* the slow rise characteristic of the water uptake of the unstressed fiber, could be detected. Thus, the reversible increase in the 490-cm^{-1} peak intensity observed in this work, and the lack of a corresponding effect on the rate of water uptake, contrasts with the decreased intensity observed at 490 and 604 cm^{-1} when the OH content increases at constant T_F.[4] It would appear therefore that no additional chemically active sites result when increased tensile stress is applied to a fused silica fiber. On the contrary, it now seems that the 490-cm^{-1} intensification is a matrix element effect associated with a structural change in existing defects. The Raman experiments involving the rate of water uptake will be described more fully elsewhere.

SUMMARY AND CONCLUSIONS

The results of a new type of experiment are presented in which high tensile stress is applied to a long fused silica optical fiber while simultaneously obtaining its Raman spectrum by forward scattering. Intensification of a sharp Raman peak near 490 cm^{-1} was observed with increasing tensile stress, and the reversible nature of the intensification contrasts with previous Raman observations in which annealing was required to produce reversibility. The Raman intensification was interpreted in terms of a decoupled local mode resulting from a stretched Si—O defect site.

[1] R. H. Stolen, J. T. Krause, and C. R. Kurkjian, Discuss. Faraday Soc. **50**, 103 (1970).

[2] J. B. Bates, R. W. Hendricks, and L. B. Shaffer, J. Chem. Phys. **61**, 1910 (1974).

[3] G. E. Walrafen and J. Stone, Appl. Spectrosc. **29**, 337 (1975).

[4] R. H. Stolen and G. E. Walrafen, J. Chem. Phys. **64**, 2623 (1976).

[5] F. L. Galeener, J. C. Mikkelsen, Jr., and N. M. Johnson, *The Physics of SiO₂ and Its Interfaces* (Pergamon, New York, 1978), p. 284.

[6] J. C. Mikkelsen, Jr. and F. L. Galeener, J. Noncryst. Solids **37**, 71 (1980).

[7] F. R. Aussenegg, M. E. Lippitsch, E. Schieffer, U. Deserno, and D. Rosenberger, Appl. Spectrosc. **32**, 588 (1978).

[8] C. M. Hartwig and L. A. Rahn, J. Chem. Phys. **67**, 4260 (1977).

[9] For initial attempts to obtain the Raman spectrum of a large stressed volume of fused silica involving examination of crack tips, see abstract of talk at 81st Annual Meeting, American Ceramic Society, Cincinnati, Ohio, 29 April–2 May 1979.

[10] Optelecom, Gaithersburg, Maryland.

[11] The value of 530-ppm OH was obtained by comparing the peak height ratio I_{3700}/I_{440} from a fiber of known OH content, with the corresponding ratio from the fibers studied here. I_{3700} refers to the Raman intensity of the OH peak at 3700 cm^{-1}. I_{440} refers to the intensity of the principal Raman peak from fused silica.

[12] T_F values were estimated by comparing the Raman peak height ratio I_{490}/I_{440} from fused silica of known T_F, with the corresponding ratio from the optical fibers studied here.

[13] G. E. Walrafen, J. Chem. Phys. **62**, 297 (1975); G. E. Walrafen and S. R. Samanta, J. Chem. Phys. **69**, 493 (1978).

[14] M. Hass, J. Phys. Chem. Solids **31**, 415 (1970).

[15] D. A. Long, *Raman Spectroscopy* (McGraw-Hill, New York, 1977), p. 143.

[16] The relaxation time is undoubtedly very much shorter than the 20–30 min required to obtain a Raman spectrum between 0 and 1100 cm^{-1}. A possible method for measuring this relaxation time by Raman techniques involves monitoring the 490- and 440-cm^{-1} peak height ratio as a function of the stretching frequency applied to the fiber by a transducer.

[17] R. A. Weeks and E. Sonder, *Paramagnetic Resonance*, Vol II (Academic, New York, 1963), p. 869.

[18] R. G. Hill and G. V. Gibbs, Acta Cryst. **B35**, 25 (1979).

[19] A. G. Revesz and G. V. Gibbs, *Proceedings of the Conference on the Physics of MOS Insulators, Raleigh, North Carolina, June* 1980, edited by G. Lucovsky (Pergamon, New York, 1980), p. 92.

[20] *Handbook of Chemistry and Physics*, 52nd ed., edited by R. C. Weast (The Chemical Rubber Co., Cleveland, Ohio, 1972), p. D-69.

- 37 -

FRACTURE OF PIEZOELECTRIC MATERIALS

R. C. Pohanka
Office of Naval Research
Arlington, Virginia

S. W. Freiman
National Bureau of Standards
Washington, D.C.

K. Okazaki and S. Tashiro
Department of Electrical Engineering
National Defense Academy
Yokosuka, Japan

ABSTRACT

This paper illustrates the relationship of microstructure, composition, and ferroelectric state, to the crack growth resistance of ferroelectric-ferroelastic materials such as $BaTiO_3$ and $Pb(Zr,Ti)O_3$ (PZT). Results of fracture energy determinations are analyzed based on predictions and observations of microcracking and twinning. Changes in the ratio of Zr to Ti in PZT for compositions near the morphotropic boundary between the tetragonal and rhombohedral symmetries are shown to have a significant effect on fracture energy. Fracture energy data in PZT are interpreted in terms of energy absorbed by a stress-induced phase transformation and by microcracking.

INTRODUCTION

At grain sizes greater than ≈ 5 μm, the fracture toughness of both $BaTiO_3$ and PZT has been shown to be significantly larger in the ferroelectric state than it is in the paraelectric state [1,2]. In $BaTiO_3$, this toughening has been attributed to the interaction of the crack with ferroelastic domains, i.e., $90°$ twins.

Variations of the fracture toughness of PZT compositions near
the morphotropic boundary between the rhombohedral and tetragonal
phases has been attributed to effects of both phase transformations
at the crack tip and microcracking [2]. Toughening of a 95-5
$PbZrO_3$-$PbTiO_3$ composition has also been hypothesized to be due to a
combination of a pressure-induced phase transformation and micro-
cracking [3]. Thus, the observed toughening in PZT and $BaTiO_3$
comes about through a number of mechanisms. The purpose of this
paper is to summarize the available information on the effects of
microstructure and composition on the strength and fracture tough-
ness of $BaTiO_3$ and PZT, and to try and assess the contribution of
each possible toughening mechanism.

EXPERIMENTAL PROCEDURE

The materials employed in this study were either obtained com-
mercially or prepared by relatively standard techniques [1,2]. The
critical fracture toughness measurements were made on center-
grooved, double cantilever beam specimens $\approx$ 38 mm x 12.5 mm x 2 mm
in size. An $\sim$ 0.5 mm saw notch served as the starting crack. The
specimens were loaded to failure by an applied moment [4] while
immersed in silicone oil at the test temperature (25 °C, ferroelec-
tric state, 150 °C, paraelectric state). The crosshead rate on the
test machine was 0.5 cm/min. The strength measurements were made
in 3-point flexure at a loading rate of 0.05 cm/min.

RESULTS AND DISCUSSION

BaTiO₃

In $BaTiO_3$ the critical fracture energy, γ, is a function of
grain size, G, in the ferroelectric state but is independent of
grain size in the paraelectric state (T_C = 130 °C) (Fig. 1). The
150 °C data fit an empirical expression:

$$\gamma = -0.02 \log G + 3.46 \qquad (1)$$

The small value of the slope indicates that γ is not a function of
grain size but remains constant at $\approx$ 3.5 J/m². Because the crystal
structure in the paraelectric state is cubic, this type of behavior
is to be expected [5]. The only deviation to this trend is the
data obtained on a ███████████, two phase material which consists
of $BaTiO_3$ and MnO_2 (grain size = 30 to 50 μm). A γ of 12.8 J/m²
was measured at room temperature compared to a value of 12.7 J/m²
measured at 150 °C on this material. Fracture analysis of this two
phase material showed the largest amount of intergranular failure
of any of the BaTiO₃ materials of comparable grain size. This
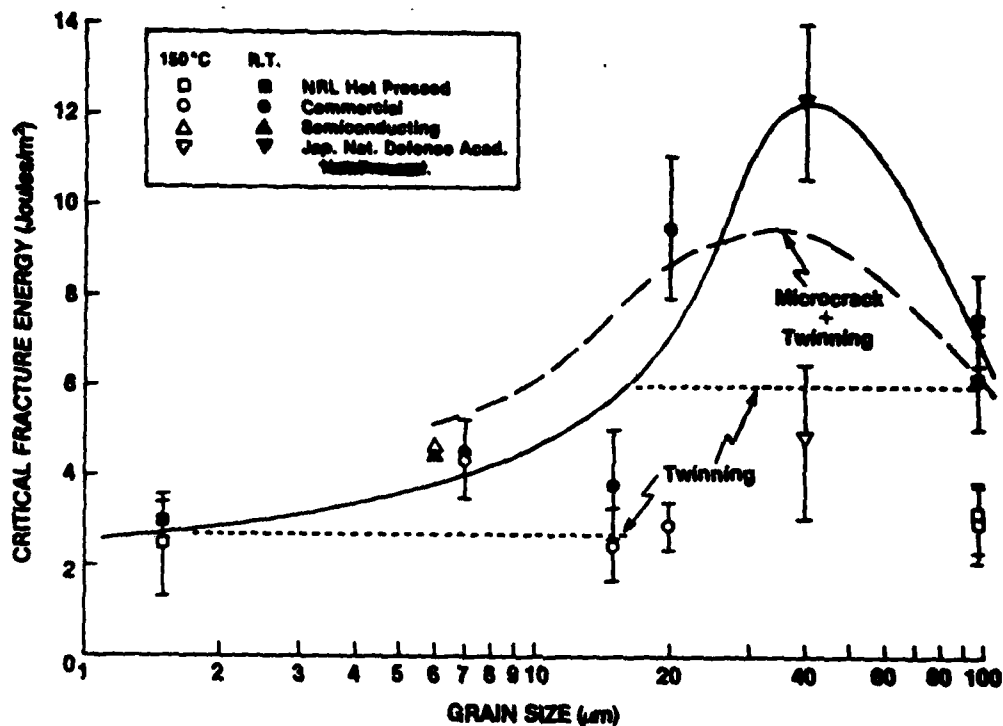difference in factor morphology suggests a different controlling

Figure 1. Fracture energy of BaTiO₃ as a function of grain
size. —— best fit to room temperature data;
... contribution due to twinning; – – – combined
effect of twinning and microcracking predicted by
Eq. 2.

mechanism for crack growth in this two phase material than in
single phase $BaTiO_3$.

The room temperature fracture energy of $BaTiO_3$, having a
tetragonal crystal structure, remains constant up to a grain size
of 15 μm, increases rather sharply then decreases (Fig. 1). This
behavior can be explained on the basis of a combination of twinning
and microcracking enhanced toughness over different portions of the
grain size range as follows.

1 to 5 μm

In the 1 to 5 μm grain size regime, ferroelastic twinning
does not occur [6], so the fracture energy of cubic and tetragonal
$BaTiO_3$ would be expected to be quite similar, as is observed.
These are the lowest values of γ, measured experimentally.

5 to 15 μm

Above a grain size of 5 μm, 90°, ferroelastic, twins are pro-
duced by the cubic-to-tetragonal phase transformation [7]. Based

- 40 -

on the increase in the fracture energy of single crystal $BaTiO_3$, from 0.8 to 1.4 J/m^2 due to the interaction of the crack with the twins, one would expect the γ of the polycrystalline materials to be increased proportionally. Increases of this magnitude are not observed in the measured values of γ. However, it is observed that fracture over this grain size range is predominantly intergranular. This means that the cracks, instead of passing through the twin structure, take the easier path around the grains. Since no crack-twin interactions take place, twinning does not influence the toughness.

It can be shown, however, that microcracking near the crack tip should affect the measured fracture energy. That microcracking must play some role in the fracture process is shown by the spontaneous cracking of polycrystalline $BaTiO_3$ at grain sizes between 150 to 250 µm [7]. Following Rice and Freiman [8], one can calculate the contribution that microcracking would make to the measured fracture energy. The measured γ can be calculated from

$$\gamma = \gamma_p \left(1 - \frac{G}{G_c}\right) + M\, \overline{\Delta\varepsilon}\, [9E\gamma_B G)^{1/2} - \overline{\Delta\varepsilon}\, EG] \qquad (2)$$

where γ_p is the fracture energy due to all contributions other than microcracking, i.e., intrinsic, twinning, etc.; G is the grain size; G_s is the grain size at which spontaneous failure occurs; $\overline{\Delta\varepsilon}$ is the average strain mismatch; γ_B is the grain boundary fracture energy; E is Young's modulus; M is an empirical constant related to the number of microcracks. Take values of these parameters for $BaTiO_3$, i.e. $E = 12.5 \times 10^{10}$ Pa; γ_B = single crystal fracture energy, 0.8 Pa-m; $\overline{\Delta\varepsilon} = 5.6 \times 10^{-4}$ based on the reduction of the higher local internal strains due to twinning [7]; γ_p = 3.5 Pa-m for G < $\approx$ 18 µm, and = 6.2 Pa-m ($3.5 \times \frac{1.4}{0.8}$) for G > $\approx$ 18 µm; G_s = 200 µm, and M = 2.5 based on the best fit to fracture energy data for a number of materials [9]. The γ calculated from Equation 1 is shown as the dashed line in Fig. 1. Considering the number of assumptions, and the experimental scatter in both the measured γ and the parameters needed to calculate it, the fit is quite good.

15 to 50 µm

Over this range, both microcracking and twinning contribute to the measured fracture energy. The maximum in the γ-grain size curve can be calculated from the following expression which is

obtained by differentiating Equation 2 with respect to G, and setting $\frac{\partial \gamma}{\partial G} = 0$.

$$G_{max} = \frac{9E\gamma_B}{4 \left(\dfrac{\gamma_p}{M\overline{\Delta\varepsilon} G_s} + \overline{\Delta\varepsilon}E\right)^2} \qquad (3)$$

Using the same values of the parameters as before, a G_{max} = 40 µm is calculated, in good agreement with the experimental value. Note that this calculation is not dependent on an empirical constant. The interaction of the twins with the propagating crack in a material having a grain size near this maximum is illustrated in Fig. 2.

50 to 200 µm

At grain sizes greater than about 50 µm, both twinning and microcracking still contribute to increased toughness, but linking of microcracks begins to occur, leading to decreasing fracture energy with grain size. The fact that the strength of $BaTiO_3$ having an average grain size of ≈ 100 µm is not lower than that at fine grain sizes [10] does not rule against microcracking. At this grain size, flaws are contained within a single grain and propagate at the single crystal fracture energy. Eventually, spontaneous failure will take place leading to a measured γ that is effectively zero.

Space Charge Effects

Since $BaTiO_3$ is an insulator at room temperature, it was thought that space charges may exist in the material, which could create additional stresses between grains. Semi-conducting $BaTiO_3$ was prepared through the incorporation of samarium in solid solution. These materials have nearly the same strains due to the cubic-to-tetragonal phase transformations but cannot maintain local space charges.

The fracture energy of a 5 to 8 µm grain size $BaTiO_3$ + Sm was 4.1 J/m^2 at 25 °C and 4.5 J/m^2 at 150 °C, in agreement with that determined on insulating $BaTiO_3$. Internal stresses calculated from the fracture energy and the flexural strength agreed with those determined in insulating $BaTiO_3$ of comparable grain size. It can be concluded that any space charges present in $BaTiO_3$ have little or no effect on fracture.
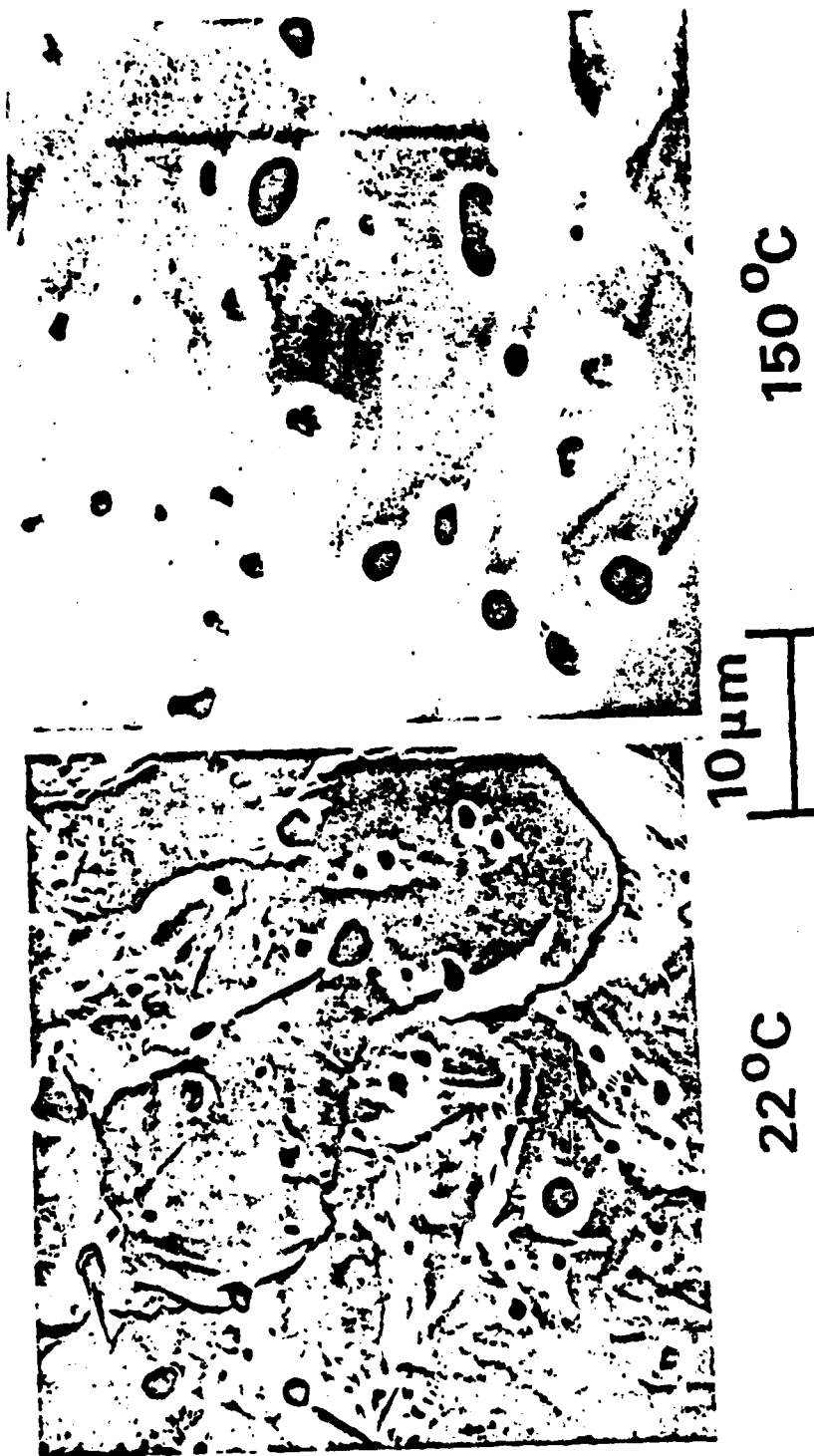
150°C   22°C

10μm

Figure 2. Microstructure of BaTiO₃ with grain size 40 μm. Note twins on the surface of the material tested at room temperature (γ = 12 J/m²) and absence of twins when tested at 150 °C (γ = 4.5 J/m²).

PZT

Table 1 summarizes the fracture energy and strength of the
PZT compositions investigated. Note that, like $BaTiO_3$, the frac-
ture energy of a commercial PZT (TLZ-H) is significantly higher in
the ferroelectric state (25 °C) than in the paraelectric (cubic)
state (200 °C). As with $BaTiO_3$, the strength of this material is
higher in the paraelectric state due to the presence of local
tensile stresses at 25 °C due to the paraelectric-to-ferroelectric
phase transformation. As seen in Fig. 3, the strength of the
material in the two states decreases and crosses with increasing
flaw size until, at some flaw size large enough to average over
the compressive and tensile components of the internal stress, the
ratio of the two strengths is essentially equal to the ratio of
$(\gamma_f/\gamma_p)^{1/2}$ as would be predicted by fracture mechanics theory.

For purer, experimental materials, there is a distinct minimum
in γ at the morphotropic boundary (53.5 $PbZrO_3$-46.5 $PbTiO_3$) between
the tetragonal and rhombohedral phases (Fig. 4). Less extensive
data obtained on a sintered PZT over the same composition range
exhibit similar variations in γ (2).

Table 1. PZT Fracture Data

Composition Pb(Zr,Ti)O_3	Crystal Structure	γ (J/m²)	Flexural Strength MPa
56	Rhombohedral	14.3	163
53.5/46.5	Mixed	6.2	68
50/50	Tetragonal	14.2	104
95/5	Rhombohedral		
As produced		11.1	58 [3]
As poled		11.1	60 [3]
Pressure Depoled		17.7	104 [3]
TLZ-H**	25 °C	4.3	81
	200 °C (paraelectric)	0.6	96

**Plessey, Australia

PZT (AUSTRALIAN)
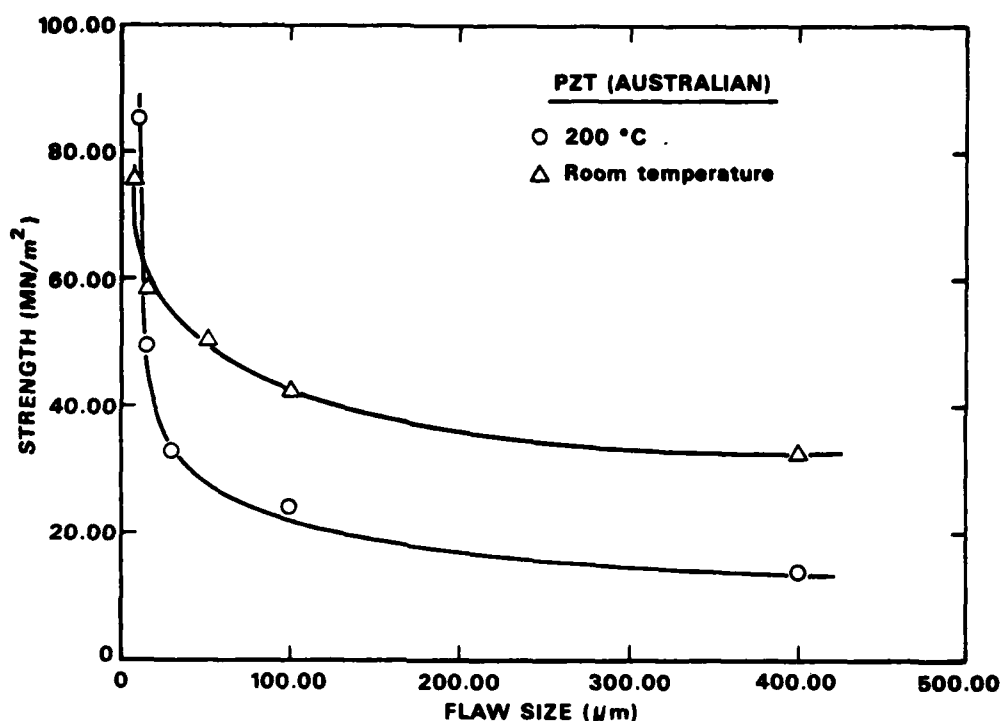
O 200 °C

△ Room temperature

Figure 3. Strength of PZT as a function of flaw size. Larger flaws were introduced by a Knoop indentor. Ratio of the strengths at a 400 μm flaw size is proportional to the ratio of $(\gamma)^{\frac{1}{2}}$ for the two conditions.

The variation in fracture energy with composition in PZT is interpreted as follows.

At the morphotropic boundary, the number of possible twin states is maximized because states for both the tetragonal and rhombohedral symmetries are permitted. Fracture is at least partially transgranular. The interaction of the crack front with the twin structure within the grains produces increased resistance to propagation in analogy with the processes in $BaTiO_3$ discussed previously. As seen in Fig. 5, the distortions in the tetragonal lattice increase with distance away from the morphotropic boundary. These strains would be expected to lead to microcracking. Two pieces of evidence for this phenomenon are the extensive cracking that occurs in $PbTiO_3$ and the hysteresis in the thermal expansion curve for the $Pb(Ti_{0.5},Zr_{0.5})O_3$ composition as reported by Biswas, et al. [11]. Similar to the analysis performed on $BaTiO_3$, one can calculate the contribution that such microcracking would make to the fracture energy of the $Pb(Ti_{0.5},Zr_{0.5})O_3$ composition. Inserting values of $\gamma_{pc} = 6.2$ Pa^{-m}, $\overline{\Delta\varepsilon} = 1.4 \times 10^{-3}$ (measured on this

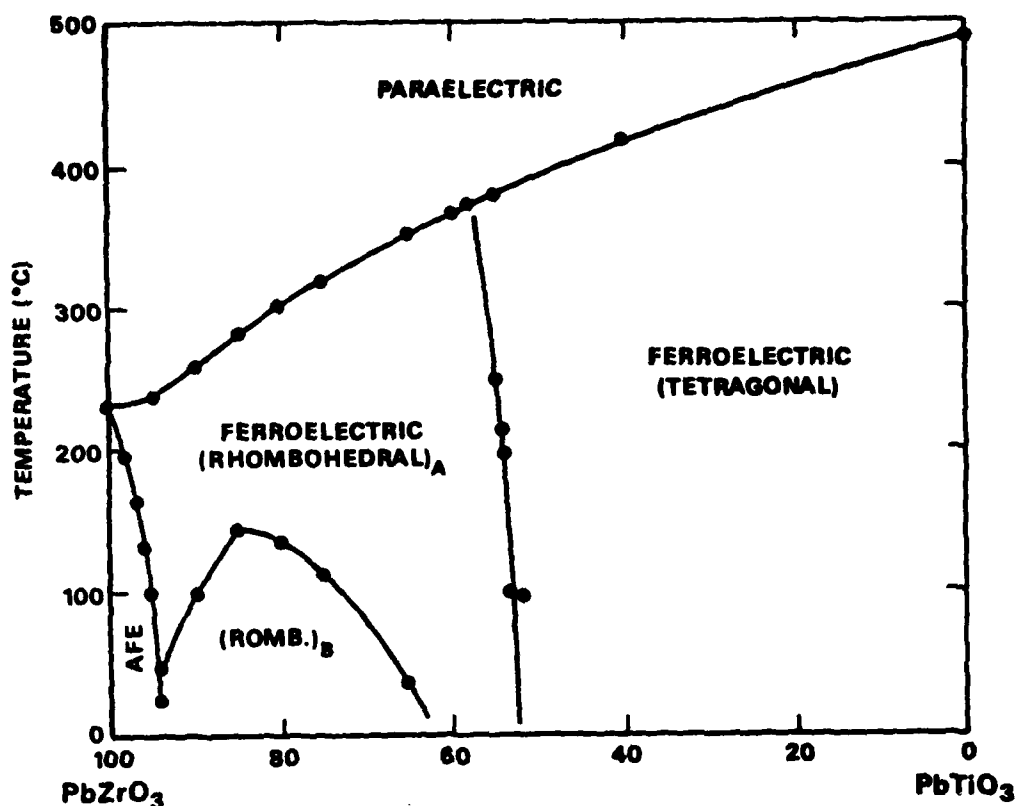Figure 4. PbZrO$_3$-PbTiO$_3$ phase diagram [7]

material), G = 200 μm, G ≈ 8 μm, E = 81 x 10^{9}Pa, γ_B = 0.6 Pa-m, and M = 2.5, into Eq. 2, one obtains a value of γ ≈ 9.4 J/m^2, somewhat less than the measured value of 14.2 J/m^2. For a constant grain size, one can also derive an expression which predicts the composition in the tetragonal phase field at which the fracture energy will be a maximum. If one assumes that the elastic modulus is constant across the composition range, one can differentiate Eq. 2 with respect to $\overline{\Delta\varepsilon}$. By setting $\frac{\partial\gamma}{\partial(\Delta\varepsilon)}$ = 0, one obtains the following expression

$$\overline{\Delta\varepsilon}_{(max \ in \ \gamma)} = 1.5 \ (\gamma_B/EG)^{1/2} \qquad (4)$$

For the values of γ_B, E, and G used previously, $\overline{\Delta\varepsilon}_{(max \ in \ \gamma)}$ = 1.4 x 10^3, essentially the strain expected for the 50/50 composition. γ is then predicted to decrease with increasing amounts of TiO$_2$.

On the other side of the morphotropic boundary in the rhombo-
hedral phase field, the lattice distortions are much smaller
(Fig. 5). This is borne out by the reduced internal stresses
measured in the 56/44 composition. Calculations of any micro-
cracking contribution to γ for this composition yields a smaller
value than that in one tetragonal state (≈ 8 J/m^2). Another mech-
anism, namely a stress induced phase transformation, may contribute
to toughening in this composition. It is expected that under a
tensile stress the rhombohedral phase in PZT can transform to the
tetragonal phase [12]. When this transformation occurs at the crack
tip, it can reduce the strains in this region and take up some of
the energy that would otherwise have gone into crack growth. How-
ever, no quantitative measure of the contribution of this mechanism
of toughening can be given at present.

Fracture data obtained on a 95 percent $PbZrO_3$ - 5 percent
$PbTiO_3$ composition (≈ 10 μm grain size) also suggest a contribu-
tion of phase transformations to toughening. In this case the
material was tested in three states, as-produced, poled, and
pressure depoled. The material that was depoled by the application
of hydrostatic compression had a fracture energy that was about 50
percent greater than that of material in either the poled or as-
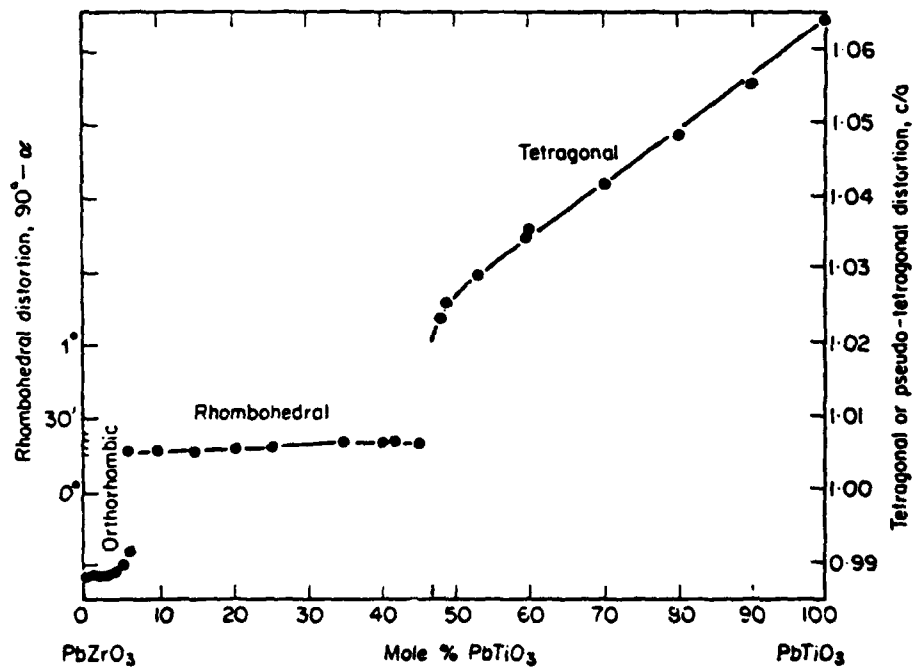produced states (Table 1). The fact that the strength of the 95/5

Figure 5.   Distortions in rhombohedral and tetragonal lattices
as a function of composition in $PbZrO_3$-$PbTiO_3$
system [7]

PZT increases after pressure depoling suggests that phase transformations play a more important role than microcracking [3]. Further evidence for phase transformation induced toughening is the reduced fracture energy of the pressure depoled material at -60 °C. No difference in γ was measured over a similar temperature range for the material in the poled or virgin states. A pressure-temperature phase diagram determined by Fritz and Keck [13] indicates that the transition from the antiferroelectric to the ferroelectric state at -60 °C extends into the tensile stress region. This shift in the ferroelectric-antiferroelectric boundary suggests that more energy would be needed to produce a phase transformation at -60 °C than at room temperature, so that the contribution of the transformation to the fracture toughness would be reduced.

CONCLUSIONS

Fracture energy data for both $BaTiO_3$ and PZT have been interpreted in terms of three different toughening mechanisms. Both twinning and microcracking were shown to contribute to the increased room temperature, fracture energy of $BaTiO_3$ for grain sizes greater than ≈ 15 µm. The grain size at which the fracture energy is maximized in $BaTiO_3$ was calculated to be 40 µm, based on a model of Rice and Freiman, in good agreement with observations.

A minimum in fracture energy was measured at the morphotropic boundary between the rhombohedral and tetragonal phases of PZT. It was hypothesized that while twinning was the major contributor to increased fracture energy at this boundary, the significantly higher γ in the tetragonal phase was due to microcracking, while the equally high γ in the rhombohedral phase was due to a stress induced phase transformation. Supporting evidence for phase transformation toughening in a 95/5 PZT was also given.

ACKNOWLEDGMENTS

REFERENCES

[1] R. C. Pohanka, S. W. Freiman, and B. A. Bender, Effect of the Phase Transformation on the Fracture Behavior of $BaTiO_3$, J. Am. Ceram. Soc. 61:72 (1978).
[2] R. C. Pohanka, S. W. Freiman, and R. W. Rice, Fracture Processes in Ferroic Materials, Ferroelectrics 28:337 (1980).
[3] J. J. Mecholsky, L. J. Storz, and J. T. Healey, Fracture Processes in Lead Zirconate-Titanate, Bull. Am. Ceram. Soc. 60: 377 (1981).

[4] S. W. Freiman, D. R. Mulville, and P. W. Mast, Crack Propagation Studies in Brittle Materials, J. Mat. Sci. 8:1527 (1973).

[5] R. W. Rice, S. W. Freiman, and P. F. Becher, Grain-Size Dependence of Fracture Energy in Ceramics: I. Experiment, J. Am. Ceram. Soc. 64:345 (1981).

[6] M. D. Dennis, Transmission Electron Microscopy of Ferroelectric Domains in Barium Titanate, Ph.D. Thesis, Pennsylvania State University, University Park, PA (1972).

[7] B. Jaffe, W. Cook, Jr., and H. Jaffe, Piezoelectric Ceramics, Academic Press, New York (1971).

[8] R. W. Rice and R. C. Pohanka, Grain-Size Dependence of Spontaneous Cracking in Ceramics, J. Am. Ceram. Soc. 62:559 (1979).

[9] R. W. Rice and S. W. Freiman, Grain-Size Dependence of Fracture Energy in Ceramics: II. A Model for Non-cubic Materials, J. Am. Ceram. Soc. 64:350 (1981).

[10] R. C. Pohanka, R. W. Rice, and B. E. Walker, Jr., Effect of Internal Stress on the Strength of $BaTiO_3$, J. Am. Ceram. Soc. 59:71 (1976).

[11] D. R. Biswas, S. Chandratreya, and J. A. Pask, Thermal Expansion, Elasticity, and Internal Friction of Polycrystalline PZT Ceramic, Bull. Am. Ceram. Soc. 58:792 (1979).

[12] L. E. Cross, private communication.

[13] I. J. Fritz and J. D. Keck, Pressure-Temperature Phase Diagrams for Several Modified Lead Zirconate Titanate Ceramics, J. Phys. Chem. Solids 39:1163 (1978).

REPORT DOCUMENTATION PAGE

READ INSTRUCTIONS BEFORE COMPLETING FORM

1. REPORT NUMBER	2. GOVT ACCESSION NO. AD-A108 045	3. RECIPIENT'S CATALOG NUMBER

4. TITLE (and Subtitle)

Stress Corrosion of Ceramic Materials

5. TYPE OF REPORT & PERIOD COVERED

Annual
1 Oct. 1980 - 30 Sept. 1981

6. PERFORMING ORG. REPORT NUMBER

7. AUTHOR(s)

S. W. Freiman, T. A. Michalske, R. C. Pohanka,
K. Okazaki, S. Tashiro, C. J. Simmons,
P. N. Krishnan and G. E. Walrafen

8. CONTRACT OR GRANT NUMBER(s)

N00014-79-F-0030

9. PERFORMING ORGANIZATION NAME AND ADDRESS

National Bureau of Standards
Fracture and Deformation Division
Washington, D.C. 20234

10. PROGRAM ELEMENT, PROJECT, TASK AREA & WORK UNIT NUMBERS

61153N, RR 022-02-01 (471)

11. CONTROLLING OFFICE NAME AND ADDRESS

Office of Naval Research
800 North Quincy
Arlington, VA 22217

12. REPORT DATE

30 Sept. 1981

13. NUMBER OF PAGES

14. MONITORING AGENCY NAME & ADDRESS(if different from Controlling Office)

15. SECURITY CLASS. (of this report)

Unclassified

15a. DECLASSIFICATION/DOWNGRADING SCHEDULE

16. DISTRIBUTION STATEMENT (of this Report)

DISTRIBUTION STATEMENT A

Approved for public release;
Distribution Unlimited

17. DISTRIBUTION STATEMENT (of the abstract entered in Block 20, if different from Report)

18. SUPPLEMENTARY NOTES

19. KEY WORDS (Continue on reverse side if necessary and identify by block number)

Crack growth
Stress corrosion
Glasses
Piezoelectric ceramics
Silica
Raman Spectroscopy
Fibers

20. ABSTRACT (Continue on reverse side if necessary and identify by block number)

A molecular model has been developed which explains stress corrosion in vitreous silica. Experiments suggested by this model showed that ammonia, hydrazine, and formamide, as well as water, enhance crack growth in silica. Crack growth studies conducted in binary soda-silica glasses in Li^+ and Cs^+ solutions show that alkali ion exchange plays an important role in crack growth. A low crack velocity plateau observed with these glasses was attributed to silica dissolution control of crack growth rates. Raman

DD FORM 1473 EDITION OF 1 NOV 65 IS OBSOLETE
1 JAN 73

S/N 0102-LF-014-6601